1-1-1972

Crystallization of polyethyleneoxide under shear.

Alfred Keith Fritzsche
University of Massachusetts Amherst

CRYSTALLIZATION OF POLYETHYLENEOXIDE UNDER SHEAR

A Dissertation Presented

By

A. Keith Fritzsche

Submitted to the Graduate School of the
University of Massachusetts in
partial fulfillment of the requirements for the degree of

DOCTOR OF PHILOSOPHY

November 1972

Major Subject: Polymer Science and Engineering

CRYSTALLIZATION OF POLYTHYLENEOXIDE UNDER SHEAR

A Dissertation

By

A. Keith Fritzsche

Approved as to style and content by:

(Chairman of Committee)

(Head of Department)

(Member)

(Member)

November 1972

DEDICATION

To Holly,

for her love and encouragement

ACKNOWLEDGMENT

I wish to thank my advisor, Dr. F. P. Price, for his encouragement and advice offered during this research. Thanks must also go to the other members of my committee, Dr. F. E. Karasz and Dr. S. Middleman, for their availability, suggestions, and constructive criticisms.

LIST OF TABLES

TABLE OF CONTENTS

CHAPTER I

INTRODUCTION

The kinetics and mechanisms of polymer crystallization and the resultant crystalline morphologies have been justifiably the focus of much scientific attention. This attention was generated not only from the intrinsic scientific interest in crystallization phenomena, but also from the fact that the properties of fabricated materials depend in large part upon the crystallinities within them. These crystallinities in turn are dependent upon the conditions under which the polymers were fabricated. The most easily altered variables are pressure, temperature, and shear rate.

Generally, polymer crystallization has been studied under a limited range of the independent variables. In the bulk, it has been studied primarily at small degrees of supercoolings, at zero shear rate, and, with the exception of the studies of Wunderlich [1-4] and a few others, at atmospheric pressure. The studies of Wunderlich concentrated primarily on thermodynamic behavior and on morphology with only minor emphasis on the kinetics of transformation under pressure.

It has been observed that the crystallization kinetics and resultant morphologies of polymers can be altered when melts are sheared or when cross-linked films are stretched.

However, most of the studies carried out on the crystallization of stressed polymer melts have been conducted under poorly defined conditions.

The purpose of this thesis is to study the kinetic behavior of stressed polymer melts by crystallizing polyethyleneoxide under well defined shear conditions. In order to study this kinetic behavior, it was necessary to design and build an apparatus with which the crystallization transformation could be observed. Once built, this apparatus was used to follow the crystallization transformation as a function of supercooling, shear rate, and molecular weight.

The plan of presentation in this chapter involves a review of the existing literature. This review will yield a basis for interpretation of the experimental results on polymer crystallization as well as a justification for this thesis. This review will concentrate on four areas: (i) the nucleation and growth theories derived from studies of quiescent systems which provide a partial basis for interpretation, (ii) the Avrami equation which provides a helpful tool with which to describe the crystallization transformations, (iii) the relationship of this thesis with studies made by other researchers, and (iv) a discussion of the theories developed to explain crystallization under stress.

Nucleation and Growth of Crystals

It has been established that when synthetic high polymers crystallize, either from dilute solution or in bulk, the processes and the resultant shapes are nucleation controlled.[5] The initiation can be either homogeneous or heterogeneous. Homogeneous nucleation results from random fluctuations of order in the melt. It is highly unlikely in comparison to heterogeneous nucleation, since it is almost, if not entirely impossible to remove all foreign nucleating artifacts from the melt. Heterogeneous nucleation results from the nucleation on the surface of these adventitious insoluble particles. Heterogeneous nucleation always occurs at lower supercoolings than does homogeneous nucleation. Therefore, heterogeneous nucleation implies a positive interaction between the surface and the newly developing crystal phase. Further, it has been shown that subsequent growth of the new layers on previously existing crystal surfaces is also nucleation controlled.[6,7]

Hoffman and Lauritzen[8,9] have theoretically treated the kinetics of polymer nucleation and crystallization in light of the work of Turnbull and Fisher.[10] The equation of Turnbull and Fisher expresses the rate of formation, both of primary and of growth nuclei:

$$I = I_o e^{-E^{\ddagger}/kT} \quad e^{-\Delta F^{*}/kT} \qquad I-1$$

I_o is an essentially temperature independent constant reflecting molecular properties and, in the case of growth nuclei, depends upon the geometry of the growth face. $E^{\pm}$ is an activation energy for transport of material across the crystal-liquid interface. ΔF^* is the work required to form the particular nucleus from the melt, k is the Boltzman constant, and T is the absolute temperature.

The critical free energy ΔF^*, which is necessary for the crystal to grow spontaneously, is given by,

$$\Delta F^* = A/ (\Delta S \Delta T)^m \qquad \text{I-2}$$

where ΔT, the difference between the crystallizing temperature and the thermodynamic melting temperature, is small. The quantity A depends on the geometry of the nucleus and the interfacial energies. ΔS is the change in entropy of melting of the polymer crystal. m is an integer. It is 1 if the process is heterogeneous and 2 if homogeneous.

For the case of a homogeneously nucleated sphere,

$$A = \frac{16 \pi \sigma^3}{3} \qquad \text{I-3}$$

σ is the interfacial energy between the surface and the melt.

If the predominant effect of shear is the alignment of portions of the polymer molecules, then this alignment might introduce an anisotropy into the melt, affecting the growth directions of the nuclei in the melt. The geometry of the nucleus might also be affected. Shear might also lower the

entropy of the melt with respect to the entropy of the crystal. This change would decrease the change of entropy of fusion of the polymer crystal.

Transformation Kinetics

The description of the transformation kinetics of polymer crystallization involves the combined effects of nucleation and growth of crystalline moieties from the melt. Several investigators have developed relationships to describe the overall crystallization transformation. Von Goler and Sachs attempted the first treatment of this type.[11] Avrami derived relationships to describe the kinetics of phase change for metals.[12-14] These relationships are presently used to describe polymer crystallization transformations. Other investigators developed relationships which are similar to those developed by Avrami and used these relationships to describe crystallization transformation in polymers.[15,16]

The Avrami equation is based upon several assumptions.

(A) It is assumed that the nuclei were randomly spaced throughout the melt. This is not true if, for instance, the walls of the container alter the nucleation of the melt.

(B) It is also assumed that the time dependence of the nucleation is either zeroth or first order. The zeroth order applies to the heterogeneous nucleation and the first order to homogeneous and sometimes heterogeneous nucleation.

Sharples showed in his studies with poly (decamethyleneterephthalate) that an induction time is sometimes necessary before all the "predetermined" nuclei can arise from the heterogeneities present in the melt.[17]

(C) It is assumed that the linear dimensions of the growing bodies are related to some integral power of time, normally the first power. In polymers this is generally true, except when the growing bodies are close to impingement.

(D) Finally, the density of the growing bodies is assumed to be constant. This is the most erroneous assumption in the derivation. It was observed that the Avrami equation applies rigorously to a system which does not change volume on transformation. Crystallization involving a relatively large volume change leads to errors of about 0.3 in the determination of the Avrami exponent.[18]

Dilatometry provides the necessary information for following the phase change from amorphous melt to crystalline polymer. In the event that the transformation goes to completion, the fraction of material transformed may be expressed by,

$$\alpha_w = \frac{V_o - V_t}{V_o - V_f} \qquad \text{I-4}$$

where α_w is the weight fraction of transformed material, V_t is the volume of the sample at any time during the

experiment, and V_o and V_f are the initial and final volumes of the sample, respectively. As the volume of the sample decreases during crystallization, a monotonically increasing sigmoidal shaped curve of α as a function of time of crystallization should result. When the transformation does not proceed to completion, this sigmoidal curve can be described in terms of Avrami kinetics as,

$$\alpha_v = F_c \left[1 - \exp(-kt^n)\right] \qquad \text{I-5}$$

where α_v is the volume fraction of the transformed material and F_c is the weight fraction of transformed material at $t = \infty$. The time the isothermal crystallization has proceeded is t and n is the Avrami exponent.

This exponent describes the combined effects of the time dependence of the nucleation process and dimensionallity of the growth crystalline moiety. A growing sphere has a dimensionallity of three. If the process is a product of homogeneous nucleation, it then has a first order time dependence. If it is a product of heterogeneous nucleation, it has a zeroth order time dependence. Therefore, the value of n is 4 for sporadic nucleation of spheres and 3 for nucleation of spheres from predetermined nuclei. However, Banks and Sharples discussed the dangers of using the Avrami exponent diagnostically to provide information of the crystallization mechanism.[19] In some instances,

the type of morphology observed by microscopy did not conform to that predicted by Avrami analysis of dilatometric data.[20] Price noted the dangers of application of the exponent to systems other than spheres, coplanar disks, or rods whose axes all lie parallel on the same straight line.[18]

The value of k, the Avrami coefficient, in the equation I-5 is given by,

$$k = \frac{4NG^3\pi\rho_c}{3\rho_a} \qquad \text{I-6}$$

for spherical growth. N is the nucleation rate, G is the linear growth rate, and ρ_c and ρ_a are the densities of the crystalline and amorphous phases, respectively. The densities are included to correct for the isovolume assumption in the derivation of the Avrami equation.

The Avrami constants are most commonly obtained from plotting ln ln $(1 - \alpha)^{-1}$ as a function of ln t. A straight line results with a slope n and an intercept k. Theory predicts that the Avrami exponent should be an integer value. However, this is frequently not the case. It is common to find non-integral values of n in the literature.[19-22]

It has also been noted that deviations from theory begin to develop toward the termination of the transformation, with the crystallization proceeding at a more protracted rate than predicted. This disparity manifests

itself above about 25 per cent crystallinity.[16]

Therefore, all interpretations of the crystallization mechanisms of polymer transformations must be made with extreme care. Attempts to deduce the mechanisms of crystallization transformations from small changes in the Avrami exponent have usually led to errors. However, large consistent differences in the Avrami exponent will serve as a basis for comparison of possible mechanisms between sheared and unsheared crystallization transformation at each shear rate and temperature over the appropriate range of crystallinities.

Stress Crystallized Polymers

Previous work by other researchers indicated that stress influences crystallization of polymers in two ways. It alters the morphology and increases the crystallization rate. This alteration in morphology can be demonstrated by contrasting polymers in dilute solutions crystallized under shear with those crystallized under quiescent conditions. The acceleration of the crystallization rate will be seen by comparison of crystallization rates of sheared and unsheared melts and cross-linked films.

When polymers in dilute solution are crystallized, the polymer chains pack into a regular lamellar array. It is accepted that the polymer chains are arranged with their backbones, c axes, in a direction perpendicular to the large flat faces of the lamellae.[23-25] The chains, which are

longer than the thickness of the lamellae, may fold back and enter the same lamella.[26]

The morphology of a single crystal can be affected by the temperature, rate of cooling, concentration, molecular structure, solvent, and substrate upon which it is grown.

The thickness of an individual lamella depends on the crystallization temperature, increasing with increasing temperature. This effect has been shown both by quenching the hot solution to different temperatures[27-29] and by crystallizing from different solvents.[30,31] If the temperature is abruptly lowered during crystallization, a small step appears on the surface of the lamellae.[27,32-34] The system appears to adjust to the new condition before an observable amount of lateral growth has occurred. The crystals continue to grow with a thickness determined by the new temperature and not by the part of the lamellar crystal already formed.

For a given molecular weight, concentration, and solvent, the morphology depends on the temperature of crystallization. One of the most comprehensive studies of the effect of temperature on morphology has been described by Bassett and Keller.[27] They used 0.01 per cent xylene solutions of Marlex 50 which were filtered at the crystallization temperature to prevent further crystal growth during cooling. At 90°C, the highest temperature at which they could grow crystals from this solution, truncated-diamond-shaped

crystals formed. They indicate that the relative size of the truncated face decreases systematically and apparently continuously as the crystallization temperature is reduced.

For a given solvent and crystallization rate, an increase in concentration leads to an increase in complexity of the resulting crystal.[26] The simplest crystals are grown from dilute solution. As the concentration is increased, twins, dendritic crystals, and numerous associated spiral growths develop. With further concentration increases, hedrites and spherulites develop.

The type of solvent used also affects the shape of lamellae. In the case of polyethylene, rhombohedral or diamond-shaped crystals can be grown from xylene,[35] tetrachloroethylene,[36] and trichloroethylene.[28] Nearly hexagonal lamellae have been found from octane[37] and decane.[26]

Molecular weight also affects crystal morphology. Till indicated that crystals become more complex with increasing average molecular weight of the polymer.[23]

The substrate on which the crystal is grown can affect its morphology. On crystalline substrates, epitaxial crystallization may occur. It has been shown that polyethylene crystallizes on freshly cleaved rock salt in the form of lamellae oriented normal to the surface.[38-40]

Lamellae were not the only structures to appear during polymer crystallization in dilute solution. Long strings of platelets, appropriately termed shish-kebobs by

Lindenmeyer,[41] have been frequent even if accidental occurrences in studies of solution grown crystals. They have their molecular direction along the shish-kebob axis and were first observed by Keller in 1959.[42] They were also fortuiously produced by Blackladder and Schleinitz by ultrasonic radiation,[43] and by Price on spraying hot solutions of polyethylene in xylene.[44] Their systematic production and investigation, however, originated from the work of Pennings and Kiel.[45] Pennings found that the shish-kebobs are readily produced when a rotary stirrer is immersed in a supercooled solution.[46] In this case, a fibrous precipitate which consists entirely of shish-kebobs, deposits on the stirrer. It has been found that a critical stirrer speed[47] or external flow rate[48] is necessary to produce this structure. Iaminar flow fields produce only precipitates such as those grown under quiescent conditions from dilute solutions. The critical stirrer speed or external flow rate is the point at which secondary flow effects known as Taylor vortices are produced. It appears that the Taylor vortices are necessary for the production of shish-kebob structures.

Pennings has also shown that the backbone forms first, and the backbone can form at temperatures which exceed the upper limit of the crystallization temperature in a quiescent solution. He has further shown that the fibrous crystalliza-

tion causes fractionation to occur. The high molecular weight material crystallizes first.[46]

The large platelets develop when the solution is cooled to room temperature after the fibrous units have already formed. The fibers then act as nuclei for the still uncrystallized molecules which then precipitate onto them, in the form of the usual chain-folded lamellae. The fibers have been obtained free of platelets by Pennings in two ways. One, when the solution is replaced by pure solvent at the temperature where the fibers have formed, the platelets have no opportunity to grow. Two, the platelets are allowed to form on cooling the precipitate together with the remaining solution and are then removed by subsequent high temperature washing such as to leave the fibers unaffected. This backbone fiber itself seems to consist of two structures. There is a 200-300 Å periodicity along the central backbone. These periodicities show up as density differences in unshadowed transmission electron micrographs. These periodicities can be converted to the appearance of the epitaxial shish-kebobs by suitable treatment with nitric acid etch or ultrasonic degradation. Removal of these ordered platelets reveals the presence of a central thread which further treatment does not alter. This central fibril is postulated to consist of highly extended polymer chains and preserves its ordered structure above the normal melting point of polyethylene.[48] This

fibrous material possesses a relatively high modulus along the fiber but a low extensibility.

During the crystallization of polymer melts under quiescent conditions, nearly symmetric structures, termed spherulites, were observed and have become recognized as the characteristic mode of crystallization of polymers from the melt. When observed after crystallization is complete, spherulites usually are polyhedral in shape, having grown radially until the entire volume is filled.[49]

When they are observed between crossed polaroids, a Maltese cross and often concentric bands appear. The Maltese cross is due to zero amplitude birefringence,[50] the vibration directions in the lamellae in the arms of the cross being parallel to the other of the polaroids. The extinction bands are due to zero birefringence[50] or very low birefringence,[51] the optic axis of the crystals in the extinguished portions of the bands being parallel to the direction of the light.

These spherulites are considered to be spherically symmetric arrays of ordered lamellae, related to the single crystals obtained from dilute solution. Not only do the polymer chains loop in and out of their lamellae, as in single crystals, but in addition the chains may traverse to adjoining lamellae or join an amorphous matrix in which the crystalline regions are embedded.

The studies of polymer crystallization under shear in the melt are neither so extensive nor so well defined as those undertaken for dilute solution crystallization under shear.

In order to determine the influence of shear on crystallization kinetics, Ashby[52] extruded and rapidly quenched lightly cross-linked melts of polyethylene from an Instron Capillary Rheometer. He differentiated between the oriented materials which were extruded at 0.05 inches/minute and the unoriented materials which were extruded at 0.002 inches/minute. Ashby heated these samples to 143°C in a sealed dilatometer long enough to melt the material but not long enough to eliminate the orientation. Next, he crystallized the extrudates at 125°C and performed an Avrami analysis upon the results. It was established that the n value decreased from 1.8 to 0.4 for the unoriented samples as the proportion of transformed materials increased. However, the oriented material showed several definite changes in the slope of the $\ln \ln(1-\alpha)^{-1}$ versus $\ln t$ plots. From a value of 1.1, n decreased to 0.5, then increased to 2.2, and finally decreased again to 0.3. Ashby concluded that the changes of the n value for the oriented material were the result of selective growth directions. An x-ray analysis of the oriented material revealed a b-axis orientation normal to the extrusion direction.

Van der Vegt and Smit[53] extruded isotactic polypropylene at 160°-180°C. Although the apparent viscosity decreased as the shear stress increased, at high shear stresses there was a point at which the viscosity made a sudden rise. Despite the fact that Van der Vegt and Smit were using temperatures from 10° to 30°C above the quiescent crystallization temperature, they attributed the sudden viscosity increases to crystallization of the melt. Unvulcanized samples of cis-1,4 polybutadiene and cis-1,4 polyisoprene were also studied yielding similar results.

Porter and Southern were able to produce a transparent, high modulus, and highly oriented filament structure from commercial high density polyethylene by crystallizing it in the Instron Capillary Rheometer under the combined influence of pressure and orientation.[54,55] X-ray analysis confirmed that the backbones of the crystalline polyethylene chains were aligned parallel to the flow axis of the rheometer.[56]

Keller and Machin[57] attempted to find the correlations of various morphologies observed for stressed crystallization conditions ranging from stirred dilute solutions to cross-linked rubbers. When stress or flow is imposed on a crystallizing polymer melt, they concluded that crystal nuclei are produced along lines parallel to the direction of stress or flow. Chain folded lamellae grow on these nuclei. Because the nucleation density along the lines is so high, only perpendicular growth is allowed. Whether the

lamellae twist as they grow to give a b-axis orientation, or grow straight out to give a c-axis orientation depends on the magnitude of the stress applied to the system. It was seen that the higher the stress, the less twisting occurred. Keller and Machin also postulated that the nucleating lines or threads were extended chains.

Keith, Padden, and Vadimsky[58,59] studied intercrystalline links and observed the fibrils running between the lamellae in quiescently crystallized polyethylene. The fibrils, according to this study, occurred when one polymer chain participated simultaneously in the formation of two lamellae. While the lamellae were being formed, the polymer chains were "reeled" into the same lattice. Based on these observations, Williamson and Bussi[60] postulated that a similar reeling-in process occurs in materials crystallizing during flow.

The mechanism of intercluster links proposed by Williamson and Bussi calls for an "elastic turbulent flow" at higher shear rates. This is produced when long chain entanglements of molecules retard the motion of molecules moving past one another. This flow then causes clusters of entangled molecules to rotate and deform as units. As the cluster rotates, the ends of the chains protruding out become enmeshed in other clusters. Therefore, extended chain crystals are formed in the middle of the chain as the two ends are reeled into separate clusters. Except for

the viscosity of the flowing medium, this appears to be analogous to the elongational flow mechanisms of Pennings' stirrer crystallized systems.

After studying the crystallization under shear of high and low molecular weight polyethylenes placed in a concentric cylinder viscomoter, Kobayashi and Nagasawa[61] observed that the induction period for crystallization decreased as the shear rate increased. The decrease in the induction period was demonstrated by an increasing shear stress. Increasing the shear rate in the high molecular weight material produced a more pronounced decline in the induction period. Pennings-type structures were observed when the inner cylinder was removed during the early stages of shear crystallization. At later stages, the crystallization of the material was found to be lamellar. The lamellae were oriented perpendicular to the flow direction. As the shear rate was increased, the orientation became along the a-axis and then c-axis. An x-ray analysis revealed a lack of crystallite orientation at low shear rates.

Patterns suggesting the formation of two different types of morphologies were observed by Keller and Hill[62] who performed x-ray studies on lightly cross-linked polyethylene as it crystallized under stress. A c-axis orientation pattern appeared first, corresponding to the fibrous nuclei previously observed. Another pattern,

suggesting chain-folded lamellae oriented perpendicular to the direction of the stress, formed and became superimposed on the c-axis orientation pattern. When melting experiments demonstrated that the second pattern disappeared before the first at a lower temperature, Keller and Hill concluded that the thread-like nuclei are not caused by heterogenieties but that they are inherent in a polymer crystallized under stress.

Haas and Maxwell[63] developed a parallel plate shearing apparatus to crystallize polyethylene and polybutene-1 melts in a polarizing light microscope. They observed that crystallization times may be several orders of magnitude less for sheared melts than those required under quiescent conditions. They also observed that the application of shear stress to an initially supercooled melt leads to a large increase in the number of crystalline structures formed and to the formation of oriented morphologies.

Wereta and Gogos[64] studied polybutene-1 which has two crystal types, hexagonal and tetragonal. Both types form directly from the melt. They found that shear increases the rate of formation of hexagonal crystals relative to the tetragonal.

Kawai, Kamoto, Ehara, Matsumoto, and Maeda[65] crystallized PET under shear in a cone and plate shearing device.

The PET was crystallized at a constant temperature at a series of shear rates, and the induction times for crystallization, indicated by increasing shear stress, were measured. The induction time decreased with shear until it reached a critical point at which the induction period increased to a maximum and finally decreased once more. DTA analysis of crystalline material showed the development of two melting peaks as the shear rate increased. One of the peaks was at a temperature lower than that observed for the unsheared material, and the other was higher. As the shear rate was increased, the lower temperature peak decreased in size, while the high temperature peak increased. Based on these results and those of x-ray, etching, and electron microscopy, Kawai et. al. concluded that the morphology was changing from chain-folded lamellae to bundle-like structures.

Baranov[66] observed that there are different morphologies in different shear domains. He believed that a low stress zone yields the growth of flattened spherulites. A higher stress zone produces structures of the shish-kebob type. The third region of yet higher stress corresponds to purely orientational crystallization.

Examination of the literature yields several conclusions about crystallization under shear stress.

I. The induction times for the appearance of crystallization are shorter under shear stress than under quiescent conditions.

II. Crystallization under shear in both solution and

melt yield different morphologies than those observed under quiescent crystallization conditions.

III. Shear alters the crystal type in polymers possessing several crystal forms.

IV. Most investigations on crystallization under shear are descriptive in nature and semi-quantitative.

Therefore, a definite need exists for a quantitative study of overall crystallization transformation kinetics of polymer melts subjected to well-defined shear stress.

Theory

Although the discussion of crystallization of natural rubbers and of cross-linked polymers has been avoided in this thesis, the theoretical considerations of Flory[67] and Krigbaum and Roe,[68] derived for these systems, are also useful in explaining the crystallization of uncross-linked melts under shear. Haas and Maxwell[63] used these theories for the interpretation of their results of crystallization of sheared polymer melts. There are many similarities between crystallization in melts under shear and that of natural rubber under stress. As in rubber and cross-linked systems, the greater the stress, the greater the orientation of the polymer chains. As predicted by Flory and Krigbaum and Roe, due to the entropy decrease associated with the alignment of the flexible polymer molecules, less entropy remains to be sacrificed in con-

verting to the crystalline state. As the material crystallizes, it behaves as a cross-linked amorphous polymer. The crystalline regions act as cross-links which are stable with respect to time, but unstable with respect to temperature.[69]

Gent[70] showed that the crystallization rate of natural rubber, like that of melts, increases as the extension ratio increases. Andrews[71] strained natural rubbers up to 300 per cent. As a result, he observed rowlike structures composed of fibrous needles perpendicular to the stretch direction and noted the disappearance of spherulitic morphology. Again, these results are reminiscent of those observed in melts under shear stress.

Flory's analysis[67] dealt with the development of an equilibrium theory to explain the effect of strain on crystallinity. Gaussian statistics and equilibrium conditions were assumed. He also assumed that crystallization occurs after the polymer has been elongated to the final relative length. Flory felt that the accelerated increase in tension with elongation and the ultimate steep slope of the stress-strain curve for crystallizing rubbers are the consequence of the cross-linking effect of the developing crystallites and the small residue of the easily deformable amorphous material at high elongations.

Based on the preceeding considerations and the assump-

tion that crystals develop only in the direction of extension, Flory developed a relationship between the degree of crystallinity of a sample, α, and the stress at a given elongation,

$$\alpha = \bar{K}\left[1 - \left(\frac{\tau}{\tau_o}\right)\right]. \qquad \text{I-7}$$

Here τ and τ_o are, respectively, the stress at which α is measured and the initial stress before crystallization begins. The value of $\bar{K}$ is given by,

$$K = \left(\frac{n}{6m}\right)^{1/2}\left[\lambda - \left(\frac{1}{\lambda^2}\right)\right] \qquad \text{I-8}$$

where m is the number of statistical segments between cross-links and λ is the elongation ratio. It will be noticed that the degree of crystallinity predicted by this equation is not a function of the crystallization temperature. It is only a function of the elongation ratio. Gent[70] showed that this analysis fits his data quite well for extension ratios greater than two. At ratios less than two, a degree of crystallinity larger than that calculated is required to reduce the stress to zero.

Flory also calculated the effect of the extension ratio on the melting point of a cross-linked system. The relationship, based on statistical mechanical considerations is given by

$$\frac{1}{T_m^o} - \frac{1}{T_m} = \frac{R}{\Delta H_m} \left[\left(\frac{6}{N_m} \right)^{1/2} \lambda - \frac{\lambda^2}{2_m} - \frac{1}{\lambda_m} \right] . \quad \text{I-9}$$

T_m^o is the equilibrium melting temperature for the unstressed sample and ΔH_m is the heat of fusion per mole of statistical segments. In the derivation of the above equation, it was assumed that the crystals developed only in the direction of extension. Flory pointed out that because of this assumption the equation does not give the correct equilibrium melting temperature at low elongations and the equation does not coverge to the equilibrium melting temperature for zero extension. Hence, the values for the melting temperature at low elongations will be too high.

Krigbaum and Roe[68] utilized x-ray analysis to study the crystallite orientation on stress crystallized samples of polychloroprene. They derived a melting point-elongation ratio equation alternate to that of Flory. It is based on free energy considerations and Gaussian statistics and yields,

$$\frac{1}{T_m^o} - \frac{1}{T_m} = \frac{R}{2 \Delta H_m N} (\lambda^2 - 2/\lambda - 3) \quad \text{I-10}$$

where N is the number of statistical segments per chain. This equation predicts the melting point at low extensions more accurately than that of Flory. However, in the derivation, Krigbaum and Roe neglected the free energy change

associated with the orientation of the crystallites formed in a stretch network. Therefore, it tends to underestimate the equilibrium melting point at higher extensions where Flory's equation works quite well.

It should again be emphasized that both the Flory theory and the Krigbaum and Roe theory are equilibrium theories pertaining to crystallization in cross-linked systems. Neither yields the kinetics of crystallization whose study is the object of this work.

In natural rubber, the chains are interconnected so that only orientation can occur upon stretching. The application of a shear stress to a melt will result in two characteristic responses. The polymer molecules can be oriented, like the chains in a network, or can slip past each other. Therefore, when a polymer melt is deformed, a portion of the energy is dissipated in viscous flow and the remainder is elastically stored.

The dynamic properties of noncrystalline entanglement networks of linear, randomly coiling macromolecules have been treated by Chompff et. al.[73,74] by modification of Rouse's bead and spring model.[75] The diffusion equation in the Rouse theory was modified by introduction of a slip parameter into the mobility-coefficient matrix to account for the slippage between polymer chains. This slip parameter can have values from zero (cross-linked molecules) to unity

(free molecules in dilute solution).

Chompff was able to determine an expression for the relaxation spectrum of an entanglement network and found that the relaxation times are inversely proportional to the mobilities of the junctions and are proportional to the square of the number of "submolecules" and to their average square end-to-end distance. The ratio of the longest finite relaxation time T^1 of a molecule with x junction points to that for a molecule with the same length but no junction points is

$$\frac{T^1}{T} = (x + 1)/L\delta \qquad \text{I-11}$$

where T is the longest relaxation time of the molecule without junction points, L is the length of the molecules, and δ is the slip parameter. If $0 < \delta < 1$ the entanglements can be considered to be more or less similar to cross-links. However, the long time region of the relaxation spectrum no longer lies at infinite time. Instead it appears at fairly long relaxation times whose position depends on the value of δ.

P. G. de Gennes[76] discussed the possible motions for one polymer molecules performing wormlike displacements inside a strongly cross-linked gel. The cross-links in the gel function as obstacles which strongly restrict the movement of the polymer chain. He felt that this approach may also be useful for the problem of entanglement effects in un-

linked molten polymers.

The crystallization kinetics of sheared polymer melts are yet unexplained by theory. The Flory and Krigbaum and Roe theories which deal with crystallization in cross-linked melts are equilibrium theories and yield no crystallization kinetics. The theories for the dynamic behavior of melts do not consider crystallinity, and even the dynamic properties of concentrated polymer solutions or melts are not well understood.

The theory is needed which deals with the crystallization kinetics of a non-crosslinked polymer melt under shear. However, consideration of the theories for dynamic behavior of molten polymers and the crystallization of cross-linked melts under stress yield several insights into the effect of shear on the crystallization kinetics as expressed by the Fisher-Turnbull equation. This equation for crystallization under quiescent conditions was discussed previously. A reexamination of equation I-1 reveals that the rate of formation of both the primary and the growth nuclei is dependent upon the activation energy for transport of material across the crystal-liquid interface, E^*, and the work required to form a particular nucleus from the melt, ΔF^*. It is also seen that ΔF^* is inversely proportional to the change in entropy of melting of the polymer crystal and the supercooling. Flory[67] has shown that when the polymer having a network structure is stretched, chains between the

network junctions are deformed from their most probable configurations. Most are elongated. Less entropy remains to be sacrificed in passing to the crystalline state, where the configurational entropy can be taken as zero. Since crystallization will occur when $T\Delta S < \Delta H_f$, the enthalpy of fusion, crystallinity may develop at a higher temperature the smaller ΔS becomes as a result of elongation. However, the elongation of an entanglement network of a melt is dependent upon the dynamic behavior of the melt. The entanglements give rise to a series of relaxation times, which are not infinite but are very long. Entanglement networks therefore do not show an equilibrium modulus but behave rubber elastically in a certain time scale. It also seems possible that these relaxation times could influence E^{+}_{-}.

Equation I-3 also shows that the critical free energy is dependent on the geometry of the nucleus and the interfacial energies. Orientation might affect this geometry, and Flory's equation worked quite well at high extensions because he assumed that the crystallites are well oriented with their fiber axes parallel to the direction of stretch.

CHAPTER II

INSTRUMENTATION

In order to build a dilatometer with which a polymer can be crystallized under shear, it was necessary to solve three design problems. One, it was necessary to design an assembly which could shear the crystallizing melt at constant shear rate over a large range of increasing viscosities with no leakage of material from the annulus. Two, it was necessary to attain a rapid thermal equilibrium in the system as well as to ascertain the temperature variation across the annulus. Temperature control and knowledge of the temperature variation across the annulus is essential due to the extreme sensitivity of polymer crystallization kinetics to the degree of supercooling. A change in one degree of supercooling may cause a change factor of ten in the crystallization kinetics. Three, it was necessary to be able to measure the volume change as the melt crystallizes. Figure 1 is a photograph of the apparatus as finally developed.

The Concentric Cylinders

The concentric cylinders are shown schematically in Figure 2. The entire apparatus was built of type 304 stainless steel except for the brass head within which the drive shaft rotates. Stainless steel was selected because

Figure 1 Concentric cylinder dilatometer assembly

1. stationary outer cylinder
2. 3/4 horsepower DC shunt-wound motor
3. reductor
4. constant diameter glass capillary
5. cathetomoter
6. thermocouple selector
7. digital read-out thermocouple thermometer
8. constant temperature bath
9. controller for constant temperature bath

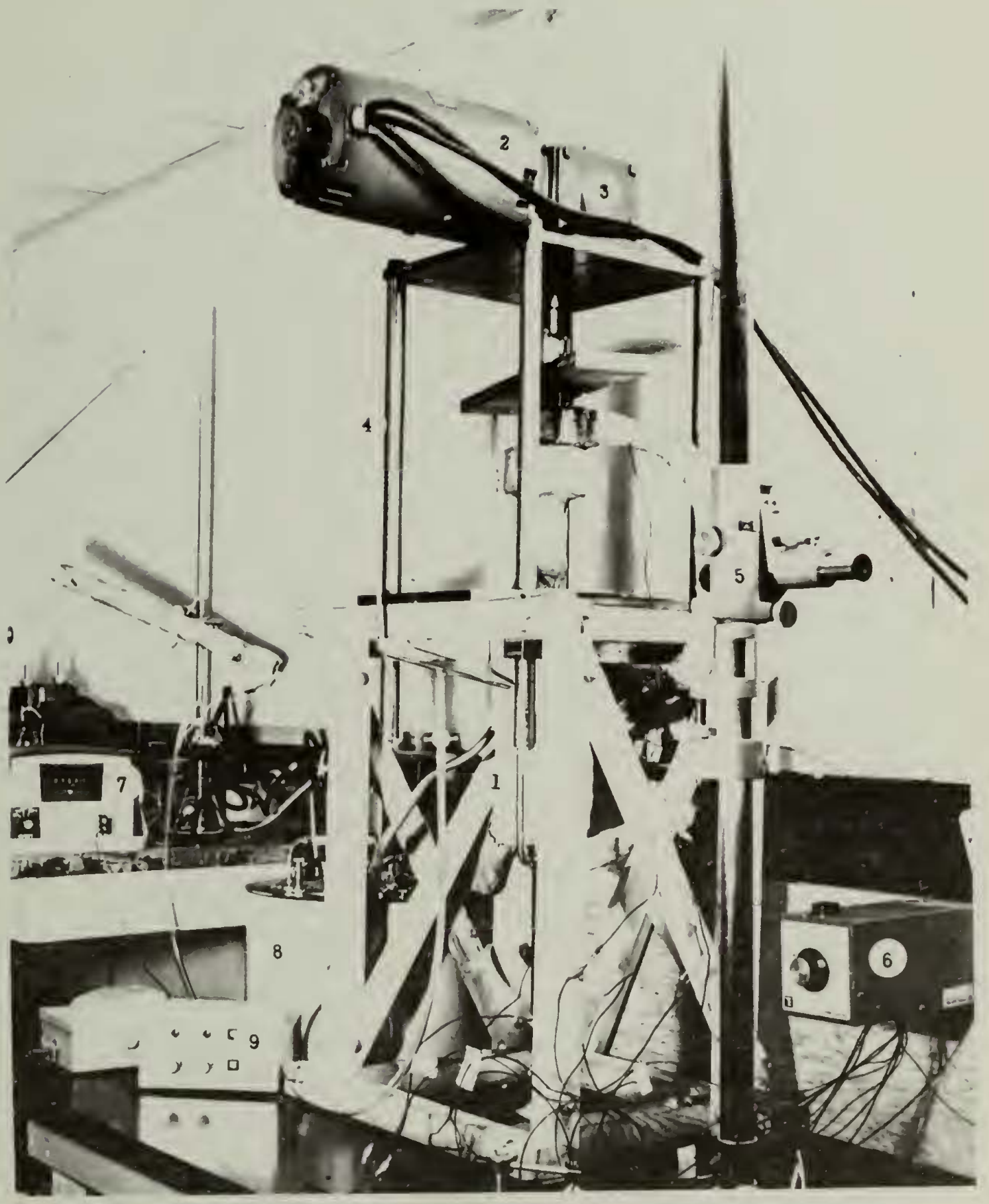
2
3
4
5
7
1
6
8
9

Figure 2 A schematic diagram of the concentric cylinders

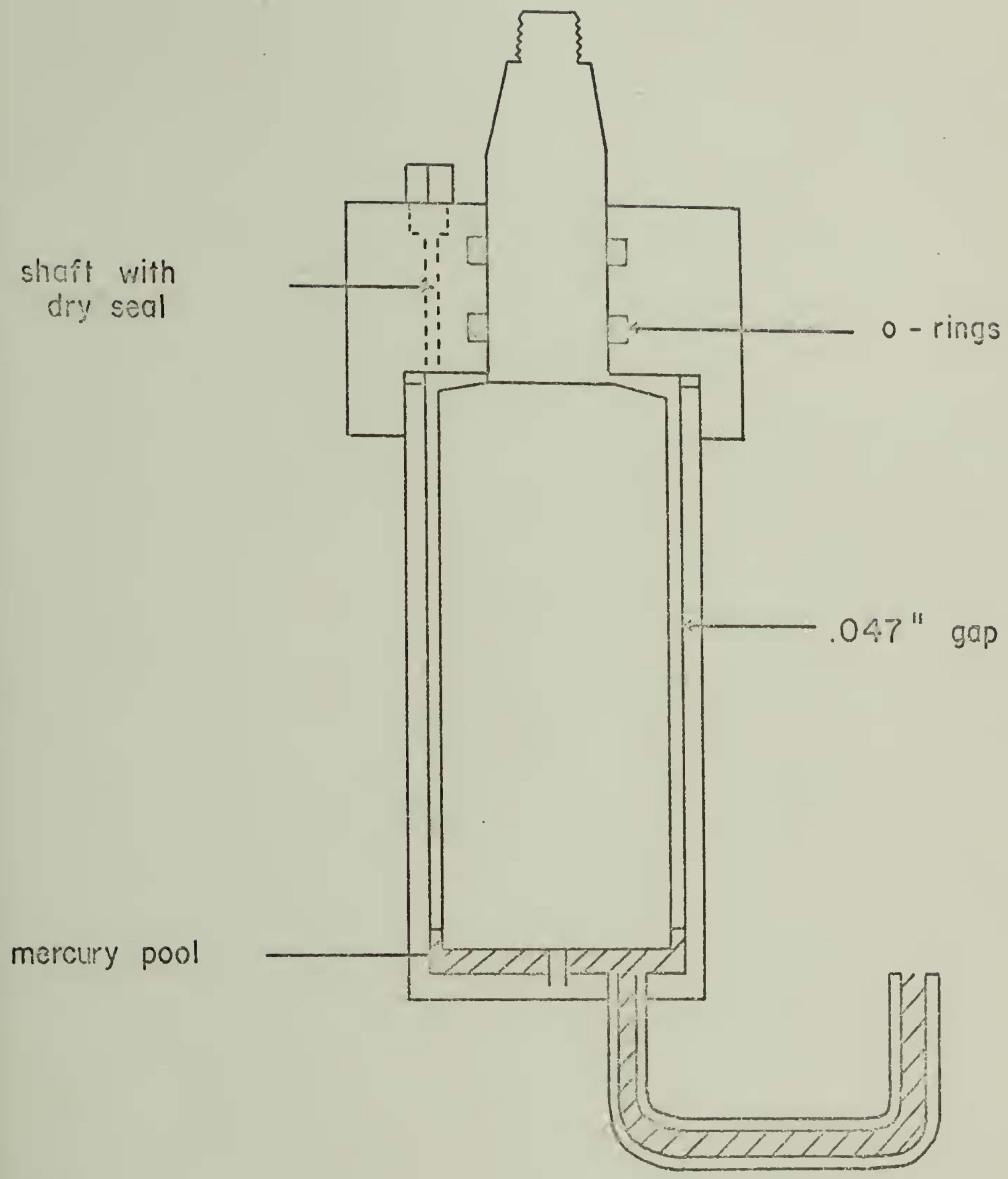
shaft with
dry seal
o - rings
.047" gap
mercury pool

it is relatively chemically inert and because it can withstand the forces generated by the high viscosities produced in the crystallization process. The head was made of brass to eliminate binding which occurs when moving stainless steel pieces are in contact. The rotating shaft is sealed by a pair of teflon o-rings mounted in the stationary head according to the roto-seal design specifications.[77] The gap between the wall is 0.047 inches (0.119cm). In order to minimize end effects on the crystallizing polymer, the upper face of the inner cylinder was cut to an angle of 35'. This is the angle which in a cone and plate viscometer gives the average shear found midway between the cylinder walls. The lower face of the inner cylinder is immersed in the mercury pool.

The polymer fills the space at the top of the inner cylinder. When using polyethyleneoxide, 35 grams of polymer is accommodated in the annulus. The space at the bottom is filled with mercury. The mercury extends into the sidearm into which a constant diameter glass capillary is inserted.

As the polymer crystallizes, the viscosity increases. Therefore a motor is needed to maintain a constant speed over a large viscosity range. A Boston Ratiotrol E75 with a motor model V9500 was selected. The 3/4 horsepower DC shunt motor has a 1750 rpm base speed. A reductor, Boston Gear model F315D, was used to reduce the speed of the drive

shaft by a factor of ten. Using this reductor, the speed of the inner cylinder may be varied from 5 rpm to 175 rpm. A shear rate variation from 15 sec^{-1} to 525 sec^{-1} can be attained.

Temperature Control

The concentric cylinder dilatometer has two heating systems. The primary system uses a constant temperature bath circulator. This system serves to bring the dilatometer to the crystallization temperature and to maintain this temperature throughout the crystallization process. The secondary system uses an electrical resistance heater to melt the polymer prior to the crystallization experiment.

In order to obtain the required temperature control in the system and the fastest possible attainment of thermal equilibrium, a Haake model NB constant temperature circulator was used with water as a circulating fluid.

The temperature in the bath can be controlled to $\pm$ 0.05°C. The water is pumped through copper coils around the outer cylinder. Thermal contact between the copper tubing and the cylinder is improved by surrounding the coils with Smooth-On, an iron filled cement which is commonly used for boiler repairs. The water is then pumped through a rotatable connection into the inner cylinder. A schematic diagram of the internal heating system is shown in Figure 3.

Figure 3 A schematic diagram of the internal heating system

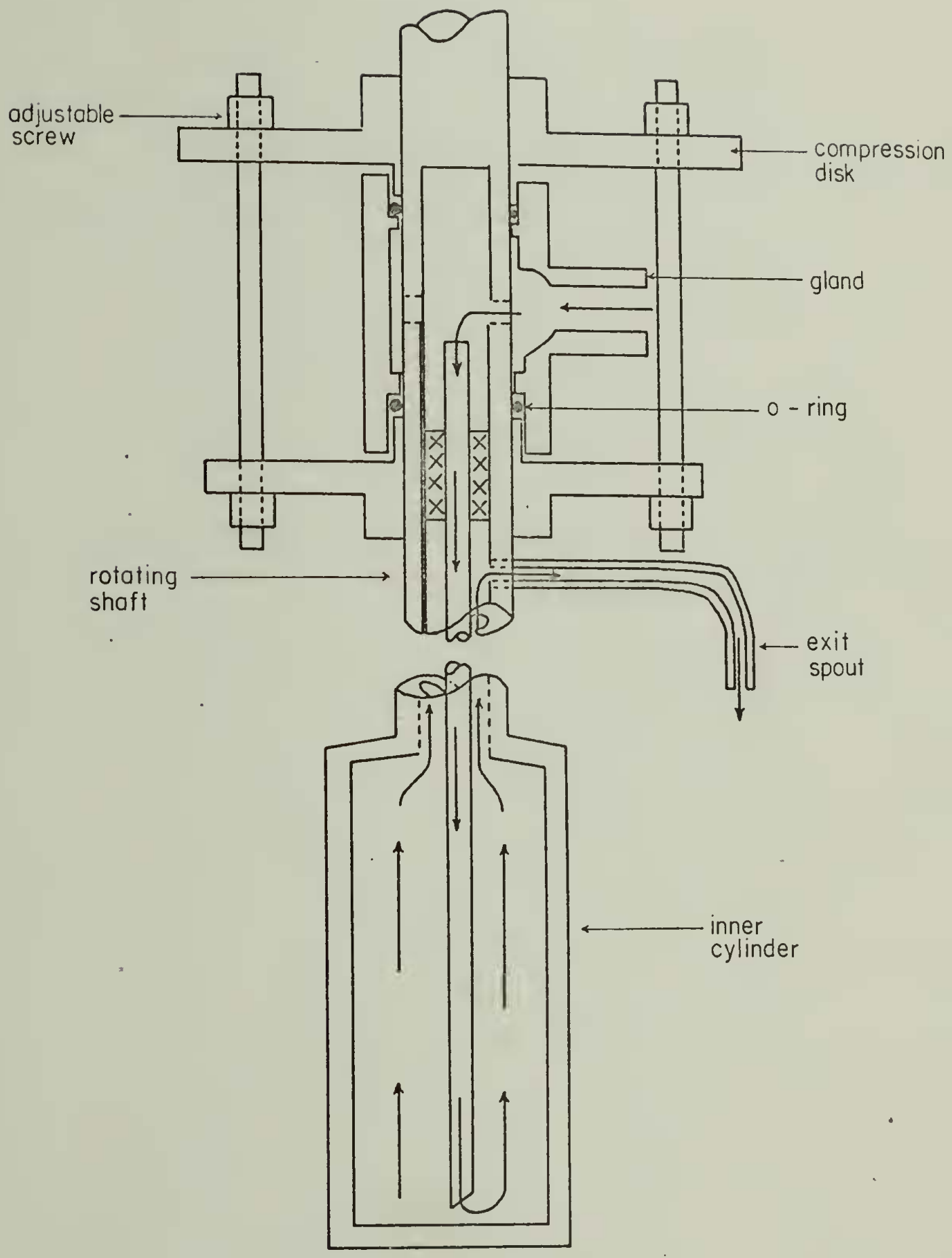
adjustable screw
compression disk
gland
o - ring
rotating shaft
exit spout
inner cylinder

the leakage of water can be minimized by adjusting the set of screws causing the disks to compress the o-rings at the top and bottom of the gland. The central tube channels the water to the bottom of the hollow rotatable inner cylinder. From there, it is forced up and out of the exit spout. The exit spout drains into a circular trough which feeds the water back into the constant temperature circular reservoir. Due to the large mass of the instrument, periods of time from fifteen to twenty minutes are necessary for the establishment of thermal equilibrium. It is therefore necessary to run crystallizations at low degrees of supercooling. This limits the range of experimental temperatures which can be used.

The copper coils which surround the stationary outer cylinder are covered with a layer of asbestos paper. Nichrome wire is would around the outer cylinder, over the asbestos paper. The Nichrome wire functions as an electrical resistance heater when current, regulated by a Variac, is passed through it. This heater is used only to raise the temperature of the system to the melting temperature prior to the crystallization experiment. It is also surrounded by a layer of asbestos.

In order to monitor the temperature of the shearing melt, thermocouples are mounted within 1/16 inch of the tips of cap screws. These screws are positioned within the wall of the outer cylinder. The tips of each make contact

with the melt. Thermocouples are also mounted between the outer surface of the stationary outer cylinder and the copper tubing and the constant temperature bath. These temperatures are monitored with a digital readout thermometer, a Digetec C-C Type T model 564.

Measurement of Volume Change

The change in volume of the polymer during the process is followed by observing the change in height in a standard constant diameter capillary of 0.110 inches diameter with a cathetometer. This capillary is seen in Figure 1. The mercury is introduced through the glass tube which contains the stopcock. This tube provides a passage for the introduction of mercury to and the removal of mercury from the system. The thistle tube mounted at the top of the capillary serves as a reservoir for any overflow of mercury when the polymer is melted at 25-30^{o}C above the crystallization temperature.

CHAPTER III

SHEAR HEATING

In the experiments described below it was assumed initially that the temperature in the sheared melt was registered by the thermocouples mounted within the walls of the stationary outer cylinder. It is known, however, that the generation of heat through the action of viscous dissipation can lead to significant variations across the shear field in the Couette configuration.

For this reason, it was deemed necessary to calculate the maximum temperature rises for Couette flow with an isothermal outer wall and either an adiabatic or an isothermal inner wall. These temperature rises are to be compared with the monitored temperature rises.

Crystallization kinetics vary greatly with small changes in temperature. Therefore, a model system was developed by computer simulation which calculated the temperature variation and the crystallization behavior at various positions across the annulus. The results of this model are used in the interpretation of the experimental results.

The equations used for these calculations were developed by Middleman[78] from the technique of Turian and Bird.[79] The maximum temperature rise assuming an isothermal inner wall is given by the following equation,

$$\Delta T_{max} = \frac{T_o B_r n^2 C_o^{1+(1/n)}}{4} \left[1 - \frac{n}{2} f(s,n) \left(1 - \frac{n}{2} f(s,n)\right)\right] \quad \text{III-1}$$

The maximum temperature rise, assuming an adiabatic inner wall, is given by,

$$\Delta T_{max} = \frac{T_o B_r n^2 C_o^{1+(1/n)}}{4} \left[1 - s^{-2/n} - \frac{2}{n} s^{-2/n} \ln s\right] \quad \text{III-2}$$

where $f(s,n) = \frac{(1 - s^{-2/n})}{\ln s}$,

$C_o = s^{2-n} (\dot{\gamma}^o/\Omega)^n$,

and $\dot{\gamma}^o = \frac{2 m \Omega}{1 - s^{2m}}$.

In these equations, T_o is the temperature at no shear, s is the ratio of the radii of the outer surface of the inner cylinder to the inner surface of the outer cylinder, $\dot{\gamma}^o$ is the shear rate, Ω is angular velocity, and n is the power law exponent. m is defined as 1/n. B_r is the Brinkman number,

$$B_r = \frac{R^{1-n} K_o V^{1+n}}{k T_o} \quad \text{III-3}$$

where R is the radius of the inner cylinder, V is the linear velocity of the inner cylinder, and k is fluid thermal conductivity. k was found in the literature[80] to be 2.916×10^4 g-cm / ^oC sec^3 for polyethyleneoxide. Ulrich[81] has demonstrated with the Weissenberg cone and plate viscometer that Carbowax 20-M exhibits Newtonian behavior over the shear

rates of interest. Under Newtonian conditions, the power law exponent n reduces to one and K_o equals the viscosity.

Only the viscosity of the melt is needed to determine the maximum temperature rises for the adiabatic and isothermal case of each shear rate. Table 1 lists the values of shear stress, normal stress, and viscosity determined for melts of Carbowax 20-M at various temperatures and shear rates. The data is derived from experimental results obtained by Ulrich on the Weissenberg cone and plate viscometer.[81]

The values of the other parameters used in solving the preceding equations are: $s = (R_i / R_o) = .9619$, $R_i = 3.016$cm., and $R_o = 3.137$cm.

Table 2 compares the temperature rises found experimentally with those found for the isothermal and adiabatic cases.

The observed rise is the difference between the temperatures monitored by the thermocouples mounted in the dilatometer when the melt is sheared and unsheared. The temperatures registered in the constant temperature bath are identical during these measurements. The temperature measured under zero shear is the base temperature. The sum of the base temperature and the observed temperature rise yields the observed temperature for each shear rate. Error is introduced into these observed values of the temperature rise by large fluctuations in ambient temperature. These fluctuations, which have varied as much as 10°C in the duration

TABLE 1

RHEOLOGICAL PROPERTIES OF CARBOWAX 20-M

T_o °C	$\dot{\gamma}$ Sec^{-1}	η Poise	Shear Stress Dynes/cm^2	Normal Stress Dynes/cm^2
58.3	28	451	12650	901.7
59.5	28	398	11970	853.1
56.0	56	437	24480	2226
57.8	56	418	23425	2130
59.1	56	396	22227	2021
58.6	84	412	34780	3658
59.8	84	389	32730	3451
60.6	84	336	32280	3404
56.6	112	428	48033	5780
58.6	112	428	45080	5422
59.8	112	389	43609	5245
60.6	112	380	42656	5131
57.1	140	403	56583	6616
58.6	140	384	53833	6295
59.2	140	376	52660	6157
60.1	140	365	51225	5996
57.8	168	366	61600	6397
59.2	168	349	58780	6103
59.6	168	341	57330	5953

TABLE 2

COMPARISON OF EXPERIMENTAL AND CALCULATED TEMPERATURE RISES FOR CARBOWAX 20-M

Measured T, °C	$\dot{\gamma}$ Sec^{-1}	Observed ΔT, °C	Abiabatic ΔT, °C	Isothermal ΔT, °C
58.3	28	.0	.08	.02
58.7	28	.0	.08	.02
59.5	28	.0	.07	.02
56.0	56	.3	.31	.07
57.4	56	.3	.30	.07
57.8	56	.4	.30	.07
59.2	56	.0	.29	.07
59.8	56	.0	.29	.07
58.6	84	.90	.66	.16
59.0	84	.50	.66	.16
59.1	84	.00	.63	.16
60.0	84	.30	.54	.14
56.6	112	1.20	1.23	.30
58.6	112	.40	1.15	.29
59.8	112	.30	1.10	.28
60.6	112	.10	1.09	.27
57.1	140	1.70	1.82	.45
58.6	140	1.30	1.74	.43
59.2	140	.80	1.69	.42
60.1	140	.60	1.65	.41

TABLE 2, Cont'd.

COMPARISON OF EXPERIMENTAL AND CALCULATED TEMPERATURE RISES FOR CARBOWAX 20-M

Measured T, °C	$\dot{\gamma}$ Sec^{-1}	Observed ΔT, °C	Adiabatic ΔT, °C	Isothermal ΔT, °C
57.8	168	2.40	2.40	.59
59.2	168	2.00	2.30	.55
59.6	168	1.20	2.22	.54

of a day, cause the temperature difference between the bath and the dilatometer to vary as much as a degree. Although the observed temperature rise values are only approximate, they are seen to lie generally between those determined for the adiabatic and the isothermal cases. This result is not unexpected. The results are not expected to correspond to the adiabatic case because the inner and outer cylinders are constructed of stainless steel, which is a fair conductor of heat. The inner cylinder is directly in contact with the circulating thermal medium. The outer stationary cylinder is in contact with the circulating thermal fluid via copper coils which are wrapped around it. Neither would the system be expected to behave exactly as predicted by the isothermal case. The walls of the inner and outer cylinders are constructed of 1/4 inch stainless steel whose thermal conductivity is only 0.107 cal/(sec)(cm^2)(^oC/cm) at 100^oC. This is approximately one-ninth that of copper and less than one-fourth that of aluminum.[82] This is a relatively low thermal conductivity and these relatively thick walls preclude the precise application of isothermal shear heating.

Model Crystallization Calculations

The previous set of calculations deals only with the maximum temperature rise as a function of shear rate in the melt prior to crystallization. In the concentric cylinder dilatometer, the temperature varies not only with radial

position and shear rate but also with the degree of crystallinity. Increases in the degree of crystallinity increase the viscosity, which, in turn, increases the shear heating. This rise in temperature will alter the subsequent crystallization kinetics. Therefore, the temperature profile and the crystallization kinetics will be altered with time. The observed gross transformation kinetics are dependent on these time dependent changes in temperature and crystallization kinetics across the annulus. It is highly desirable to design a model system which allows the computation of these changes in temperature and crystallization as a function of both radial position and time. The gross transformation kinetics, calculated from the model, will aid in the interpretation of the experimentally determined gross transformation kinetics.

In order to calculate, as a function of time, the temperature and crystallization profiles across the annulus, it is necessary to determine four quantities; the fraction of crystallinity, the density, the viscosity, and the temperature at each position and time. Each is related to and dependent on the others.

It is assumed that the fraction of crystallinity is given by the Avrami equation,[12-14]

$$X_c = 1 - e^{-kt^n} \qquad \text{III-4}$$

where X_c is the fraction of crystallinity, k is the Avrami coefficient, t is the time, and n is the Avrami exponent.

The quantity, k, is a function of the shape of the crystalline moieties, the nucleation rate, the degree of supercooling, and the shear rate. The change with temperature of the experimentally determined values of the Avrami coefficients for sheared melts of Carbowax 20-M is used to obtain the temperature coefficient of the Avrami coefficient with shear rate is assumed to be small in comparison with its temperature dependence. Therefore, the shear rate dependence of the Avrami coefficient is neglected. The Avrami exponent, n, is arbitrarily set equal to 3.0.

The required expression for the viscosity as a function of crystallinity is taken as,

$$\eta\ (X_c) = \frac{\tau_o}{\dot{\gamma}} + \frac{\left(\frac{\Delta T}{\Delta X_c}\right)(X_c)}{\dot{\gamma}} \qquad \text{III-5}$$

where τ_o is the melt shear stress, $\dot{\gamma}$ is the shear rate, and η is the viscosity. This equation is developed from the stress and crystallinity data of Wereta and Gogos.[64] A value of 2.74×10^{-5} dynes/cm^2 / 100% crystallinity for $\Delta T/\Delta X_c$ is estimated from data presented in the same paper. The change in viscosity with temperature is so small in comparison to the change in viscosity with crystallinity that this change with temperature is neglected. This value of the viscosity is needed in the calculation of the temperature at various positions across the annulus. The temperature as a function of position is assumed to be given by,

$$T = T_b + \frac{n\dot{\gamma}^2 R^2}{4k}\left[1 - \left(\frac{m\Delta r}{R}\right)^2\right] \qquad \text{III-6}$$

where R is .119cm, the annular distance; m is an increasing integer, 0,1,2...; Δr is the increment distance; k is 2.916×10^4 g-cm/°C-sec^3, the fluid conductivity; and T_b is the bath temperature.[83]

The density, ρ, is also calculated as a function of time and temperature by the equation,

$$\rho = \rho_a (1 + \beta \Delta T) + (\rho_c - \rho_a) X_c \qquad \text{III-7}$$

where ρ_a is the density of Carbowax 20-M melt (1.083 g/cm^3 at 80°C),[80] β is the change in density with temperature ($-.490 \times 10^{-3}$ g/cm^3°C),[84] and ρ_c is the density of crystalline Carbowax 20-M (1.33 g/cm^3).[85]

The distance across the annulus is divided into n parts of equal distance ΔX. The distance of any position under consideration from the rotating inner cylinder is given by $m\Delta X$ where m is an increasing integer varying in steps of one from zero to n. The times of the calculations are also equal increments of Δt starting with m = 0.

The program starts at m = 0 for ΔX and Δt. The fraction of crystallinity is also set equal to zero. The viscosity is first calculated. The calculated value of the viscosity is then used to calculate the temperature rise resulting from shear heating. Knowing the temperature at this position, the density may be calculated. The results of the above cal-

culations are then used to calculate the fraction of crystallinity at the next time interval. This value allows for the viscosity, temperature, and density to be derived in turn. The process is repeated for increasing m until m equals n. Then the calculations are repeated at the next annular position. In this manner, profiles of the fraction of crystallinity, density, temperature, and viscosity at each time and position are obtained. The average fractional crystallinity, the average density, the average temperature, and the average viscosity across the annulus at each time are also computed. The temperature profile of Carbowax 20-M sheared at 168 sec^{-1} with a bath temperature of 57.0 ^{o}C is shown in Figure 4. A temperature difference of approximately 1.2 ^{o}C exists between the rotating inner cylinder, assumed adiabatic, and the stationary outer cylinder, which is assumed to be at the temperature of the bath. Figure 5 is the profile of the fraction of crystallinity versus radial position of this high shear rate. It can be seen that when the polymer crystallization has this high dependence on the supercooling that almost no crystallization occurs at the rotating inner cylinder. Most of the crystallization occurs near the walls of the stationary outer cylinder. With this increase in degree of crystallinity, there is concomitant increase in the viscosity and temperature at these positions. There is a much more rapid rise in the temperature closer to the outer

Figure 4 A profile of the temperatures versus the distances from the rotating inner cylinder of Carbowax 20-M sheared at 168 sec^{-1} at various times.

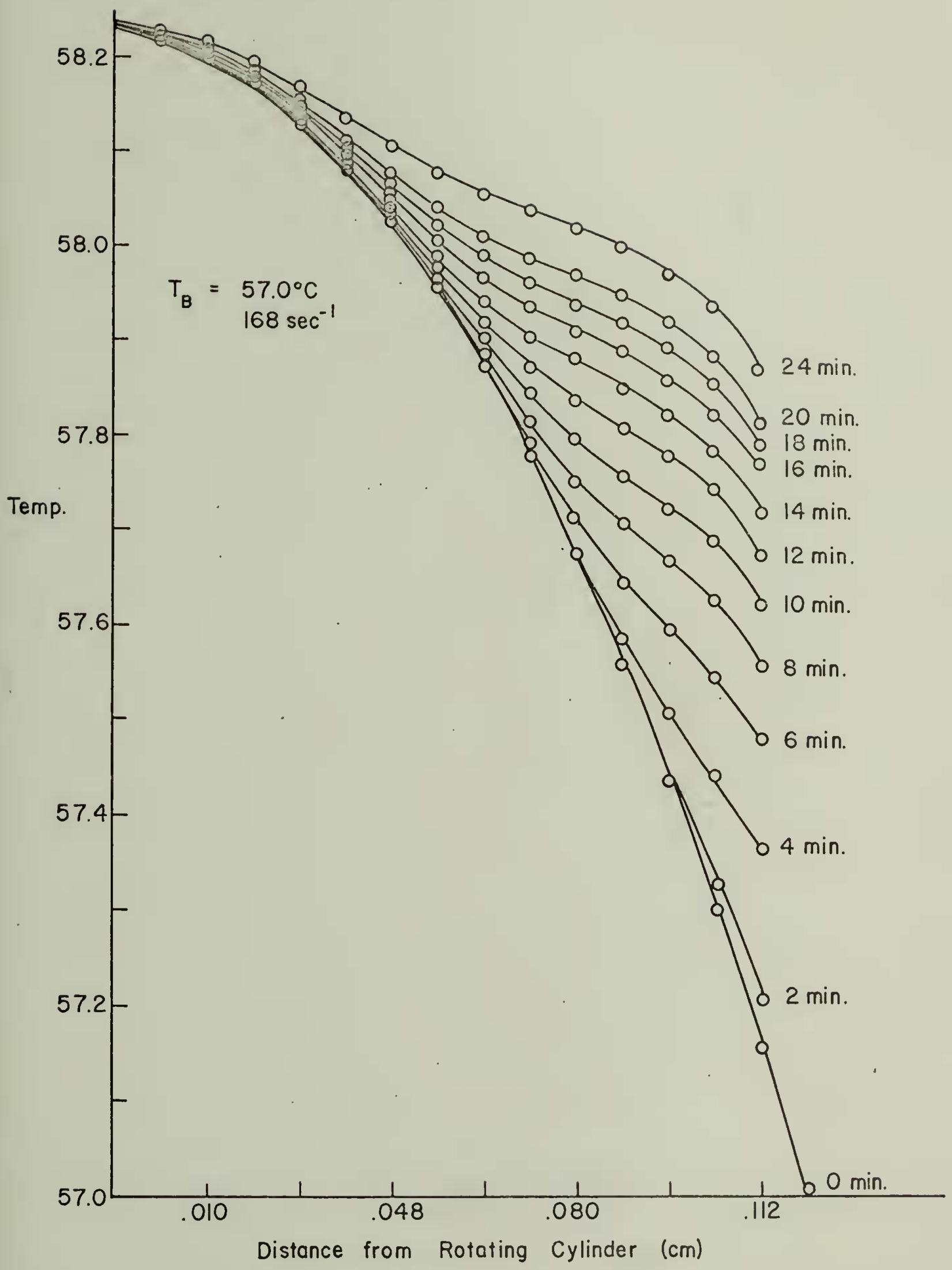
58.2
58.0
57.8
57.6
57.4
57.2
57.0
Temp.
T_B = 57.0°C
168 sec^{-1}
24 min.
20 min.
18 min.
16 min.
14 min.
12 min.
10 min.
8 min.
6 min.
4 min.
2 min.
0 min.
.010
.048
.080
.112
Distance from Rotating Cylinder (cm)

Figure 5 A profile of the fractions of crystallinity versus the distances from the rotating, adiabatic inner cylinder for Carbowax 20-M sheared at 168 sec^{-1} at various times

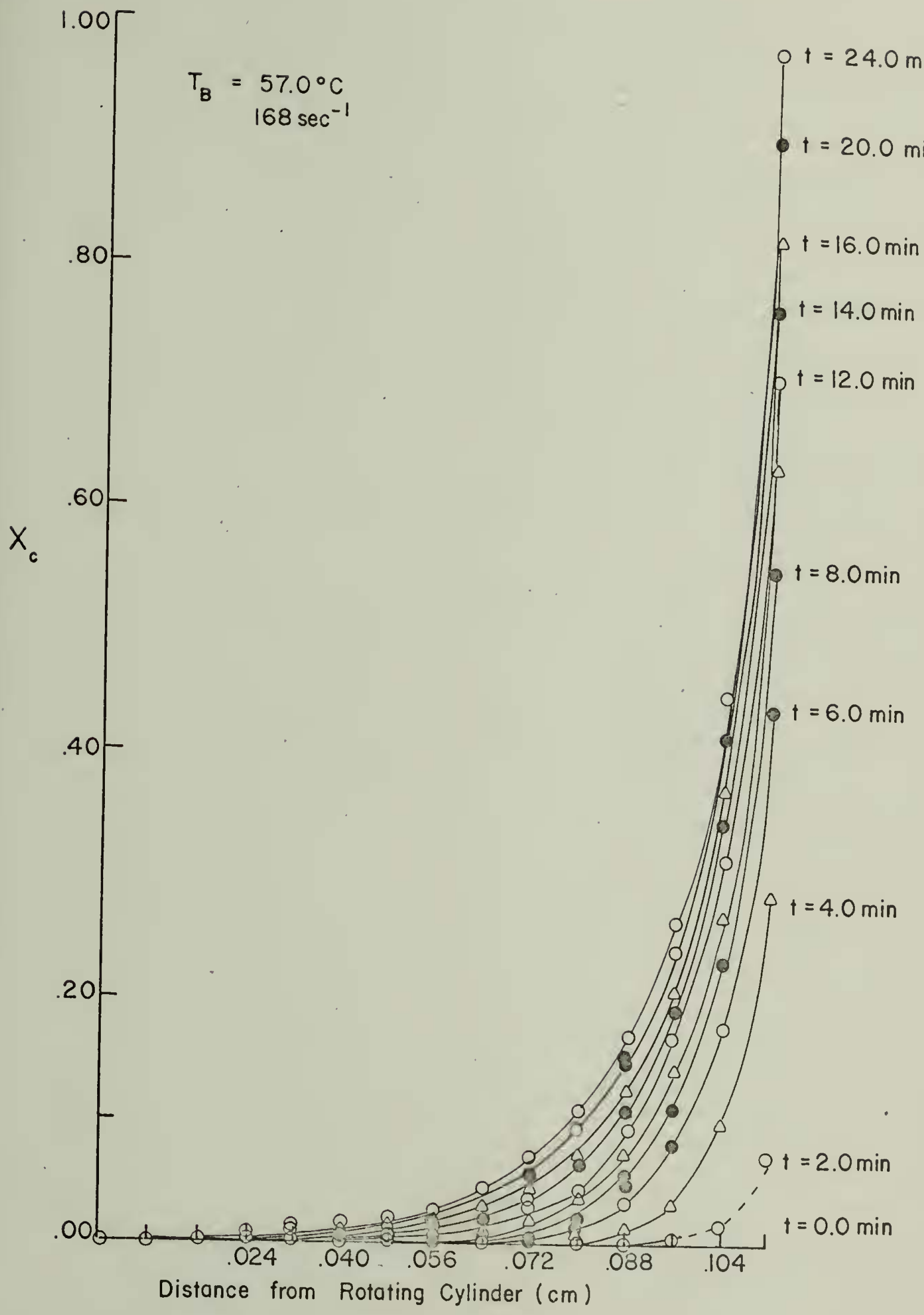
1.00
.80
.60
.40
.20
.00
X_c
T_B = 57.0 °C
168 sec^{-1}
t = 24.0 min
t = 20.0 min
t = 16.0 min
t = 14.0 min
t = 12.0 min
t = 8.0 min
t = 6.0 min
t = 4.0 min
t = 2.0 min
t = 0.0 min
.024
.040
.056
.072
.088
.104
Distance from Rotating Cylinder (cm)

cylinder than closer to the inner cylinder. Therefore, the average temperature across the annulus approaches the maximum temperature. Figure 6 is the crystallization profile of Carbowax 20-M at the much lower shear rate of 28 sec^{-1} with a bath temperature of 57.5 ^{o}C. In this case the temperature variation across the annulus is .038 ^{o}C at zero minutes and .327 ^{o}C at 18 minutes. Although there is variation of the degree of crystallinity with radial position, it is not so extreme as in the more highly sheared crystallization profiles.

The average degree of crystallinity across the annulus can be used to determine the Avrami constants. These determined values can be compared with the values originally used in the calculations. Any changes observed in the derived Avrami constants in comparison with the original values will aid in interpreting those values calculated from the experiments. The Taylor's series expansion of the Avrami equation is

$$1 - X_c = 1 - kt^n. \qquad \text{III-8}$$

This equation is valid at low fractions of crystallinity and has a 5% error in the calculated degree of crystallinity at a 10% degree of crystallinity. This equation reduces to

$$X_c = kt^n$$

which in logarithms is

$$\ln X_c = \ln k + n \ln t.$$

Figure 6 A profile of the fractions of crystallinity versus the distances from the rotating inner cylinder for Carbowax 20-M sheared at 28 sec^{-1} at various times

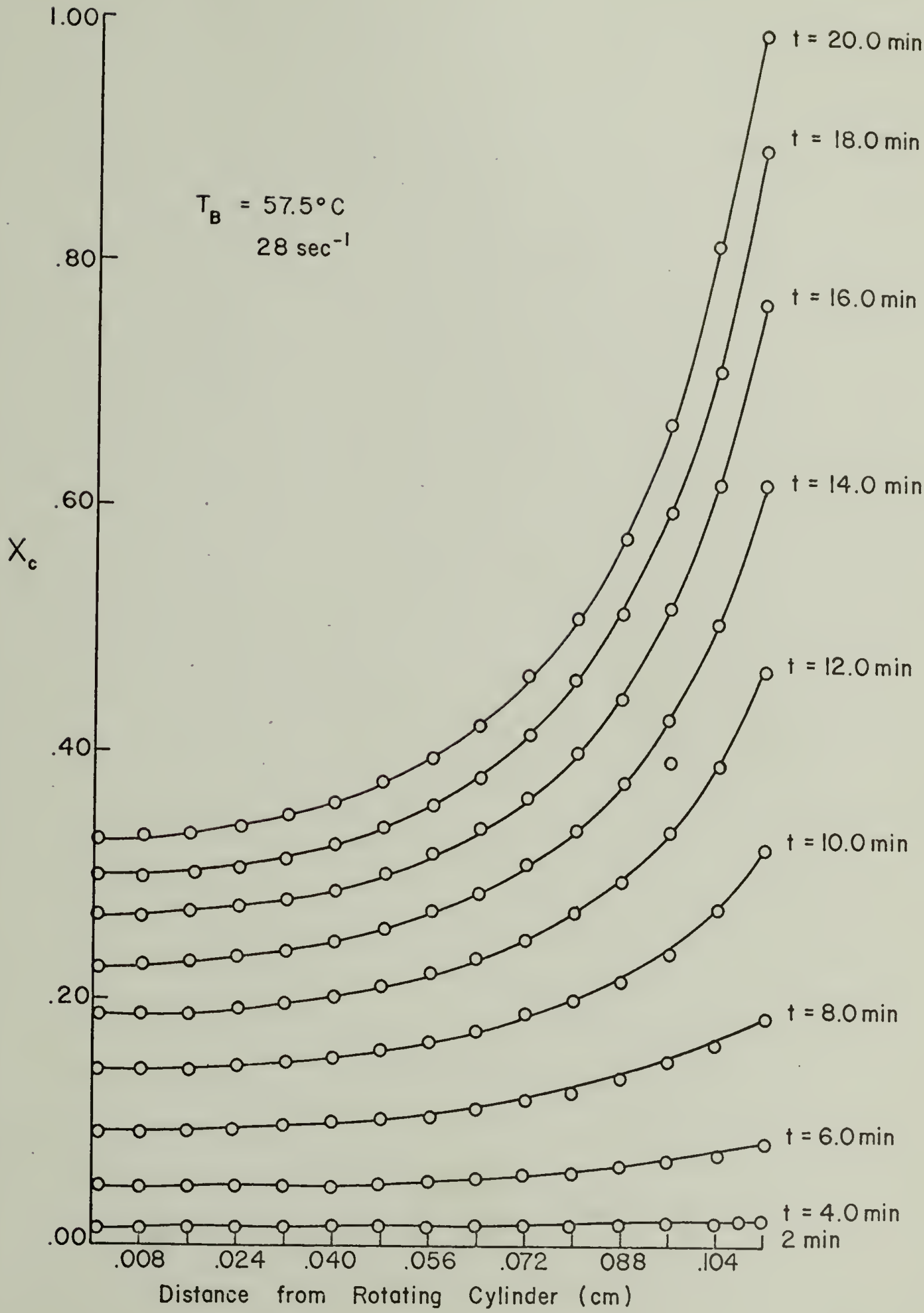
1.00
.80
.60
.40
.20
.00
X_c
T_B = 57.5°C
28 sec^{-1}
t = 20.0 min
t = 18.0 min
t = 16.0 min
t = 14.0 min
t = 12.0 min
t = 10.0 min
t = 8.0 min
t = 6.0 min
t = 4.0 min
2 min
.008
.024
.040
.056
.072
088
.104
Distance from Rotating Cylinder (cm)

This equation has the form

$$y = a + bx$$

and yields a straight line when the fractions of crystallinity versus time are plotted on log-log paper. If the temperature of the melt were constant across the annulus, the slope of this straight line would be 3.0. This is the value used for the Avrami exponent in these calculations.

When the calculated average degrees of crystallinity are plotted logarithmically against the logarithms of time, the lines are linear only at low fractions of crystallinity, and their slopes are less than the Avrami exponents used in the calculations. For example, the linear portion of the calculated crystallization curve at 56 sec^{-1} shear extends only to about $X_c = .12$ and yields an $n = 2.75$. For 28 sec^{-1}, the calculated curve deviates from linearity at $X_c = .15$ and has $n = 2.87$. The deviation occurred at $X_c = .03$ for the model at 168 sec^{-1} shear. Above these fractions of crystallinity the slopes become less and less with increasingly negative curvature. The negative curvature increased with increasing shear rates, and departures from linearity appeared at lower degreees of crystallinity with increasing shear rates.

This model study emphasizes several limitations on the experimental results from the dilatometer. Useful crystallization data can only be obtained at low fractions of crystallinity. The values of the Avrami exponent obtained

from these experiments represent only minimum values. The calculated Avrami coefficients diminish in accuracy and reliability as the shear rate is increased. Therefore, the best results will be obtained from the lowest possible shear rates at the beginning of the crystallization transformation. The largest fraction of the total crystallization should occur nearer the cooler, stationary outer wall. So, a thermocouple mounted at this wall surface should give the most accurate representation of the crystallization temperature. It was also observed that increasing the temperature of the bath at constant shear rate does not alter the temperature or crystallization profiles. It only changes the time of appearance of each respective profile.

CHAPTER IV

EXPERIMENTAL

Preparation of Sample and Instrument

It is imperative to remove any air from the polymer melt. Air has a very high coefficient of thermal expansion and a high coefficient of compressibility. The coefficient of compressibility is particularly important because small changes in the height of mercury in the capillary will alter the pressure on any air bubbles in the melt. A concomitant expansion of these bubbles with decreasing mercury height would complicate the interpretation of the experimental results. Therefore, the polymer is melted and held under a vacuum for twenty-four hours to remove all the air bubbles prior to its introduction into the dilatometer.

A known amount of the melt is poured onto a mercury pool at the bottom of the outer cylinder. The melt crystallizes on top of the mercury pool during this step. The cylinder is mounted and partially screwed into the stationary head. Then the resistance heater is activated in order to remelt the polymer. The outer cylinder is then tightly screwed into the stationary head, and the capillary system is added. The connection between the male joint of the capillary system and the female joint on the sidearm is sealed with high vacuum wax in order to prevent the leakage

of mercury through this connection.

More mercury is introduced into the capillary system through tygon tubing connected to the intake tube. The pressure exerted by the mercury forces the polymer into the vacant region between the two cylinders. The air is forced out the dry seal shaft. When melt appears in this shaft, the chamber is filled, and the dry seal is replaced.

Calibration

In order to determine the fraction of crystallinity as a function of time, it is necessary to know the total change in height of the mercury from the crystalline phase to the melt at the temperature of interest. This change of height and the coefficients of thermal expansion for the melt and mercury and crystalline and mercury phases are obtained from a calibration curve as shown in Figure 7 for a sample of polyethyleneoxide. Such a curve must be constructed for each new sample placed in the dilatometer. The curve is constructed by heating the sample in steps and recording the height of mercury at each temperature. Twenty-four hours are allowed for each temperature increment to insure the establishment of equilibrium. In this manner, the entire melting range is traversed. The temperature of melting is also obtained from this curve. The reduced crystallinity may be directly determined by changes

Figure 7 Calibration curve for a sample of polyethylene-oxide, the height of mercury in the capillary plotted against the temperature

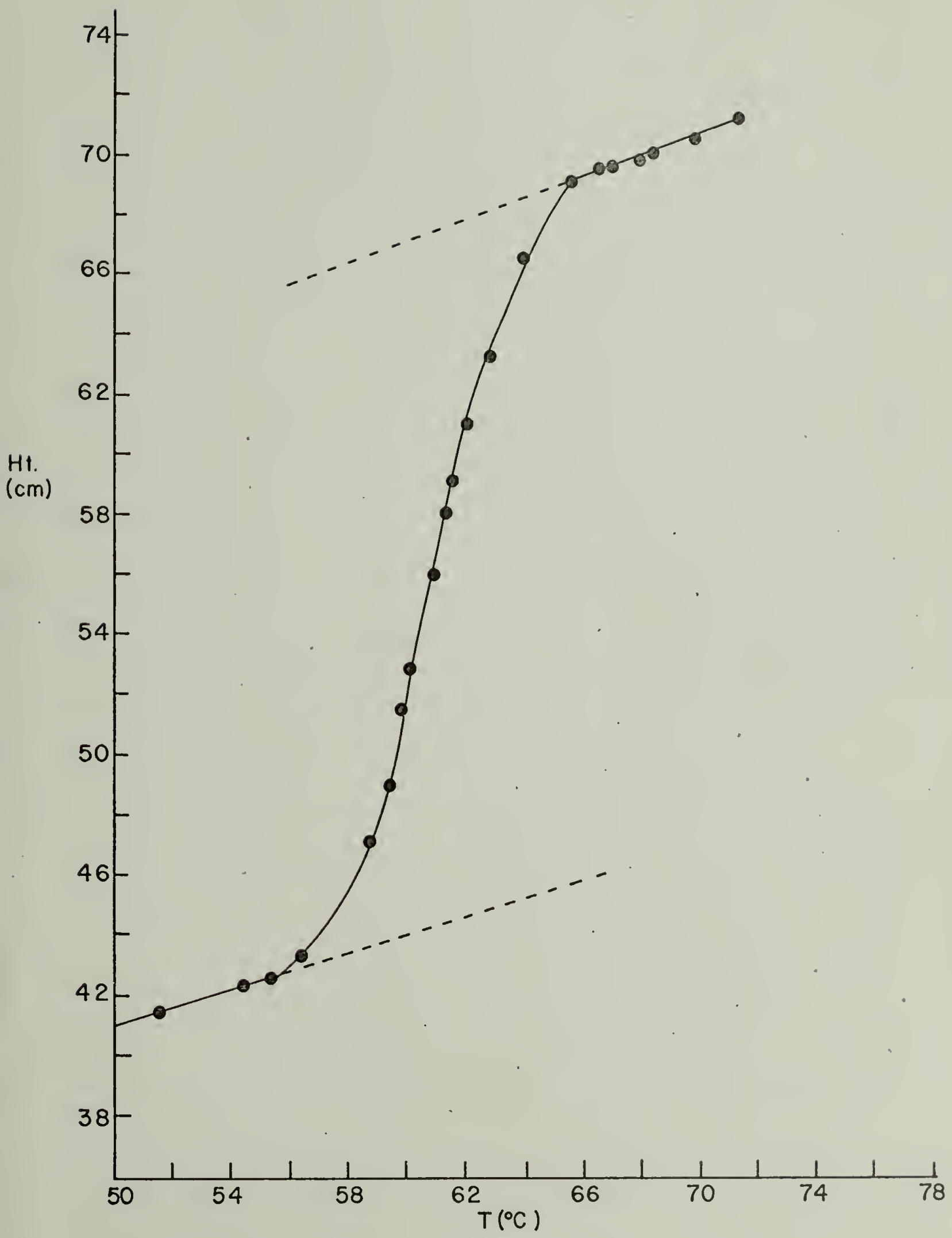
74
70
66
62
Ht.
(cm)
58
54
50
46
42
38
50
54
58
62
66
70
74
78
T (°C)

in the height of mercury as a function of time for the crystallization experiment by,

$$X_r\ (t) = \frac{H_a - H\ (t)}{H_a - H_c} \qquad \text{IV-1}$$

where X_r (t) expresses reduced crystallinity as a function of time, H_a is the height of mercury at temperature T prior to crystallization, H_c is the height of mercury upon completion of crystallization at temperature T, and H (t) is the height of mercury at any time at temperature T during crystallization.

The fraction of crystallinity may then be obtained by,

$$X_c\ (t) = (F_c) \cdot \left[X_r\ (t)\right] \qquad \text{IV-2}$$

where X_c (t) is the fraction of crystallinity as a function of time, X_r (t) is the reduced crystallinity as a function of time, and F_c is the fraction of crystallinity in a completely transformed sample.

Procedure

Each crystallization experiment is run according to an identical procedure. The electrical resistance heater is activated and the polymer is heated to thirty degrees above its melt temperature. The polyethyleneoxide samples were heated to 95°C. This heating insures the melting of all the crystalline aggregates in the melt and the lapse of the polymer memory in the melt. The electrical resistance heater is then turned off and the temperature is

allowed to fall under the influence of ambient temperature to ten degrees above the melting temperature. Usually it takes about thirty minutes for the temperature to fall from 95^{o} to 75^{o}C for polyethyleneoxide. The motor is then activated at the desired speed. After the temperature has fallen another five degrees, the constant temperature circulator is started. The temperature and height of mercury in the capillary are then recorded at regular intervals. Figure 8 is the crystallization curves for Carbowax 20-M crystallized at 56 sec^{-1} at 59.1^{o}C and at 59.6^{o}C. The solid circles and triangles are the height of mercury at each time interval while the open ones are the temperature at each time interval. A rapid drop in the temperature and the height of mercury is initially observed. The height of mercury and the temperature become constant until the crystallization starts. Then the height of mercury falls. The time at which the temperature of the system reaches equilibrium is defined as the starting time of the experiment (t_0). An error of several minutes in determining the starting time yields a corresponding error in the induction time at high degrees of supercooling. This uncertainty in turn gives errors in the shapes and positions of the crystallization curves derived from them. This uncertainty diminishes with smaller degrees of supercooling.

Figure 8 The height of mercury and the temperature plotted versus time for Carbowax 20-M crystallized at constant shear rate (56 sec^{-1}) and at the temperatures of 59.1 ^{o}C, the triangles, and 59.6 ^{o}C, the circles.

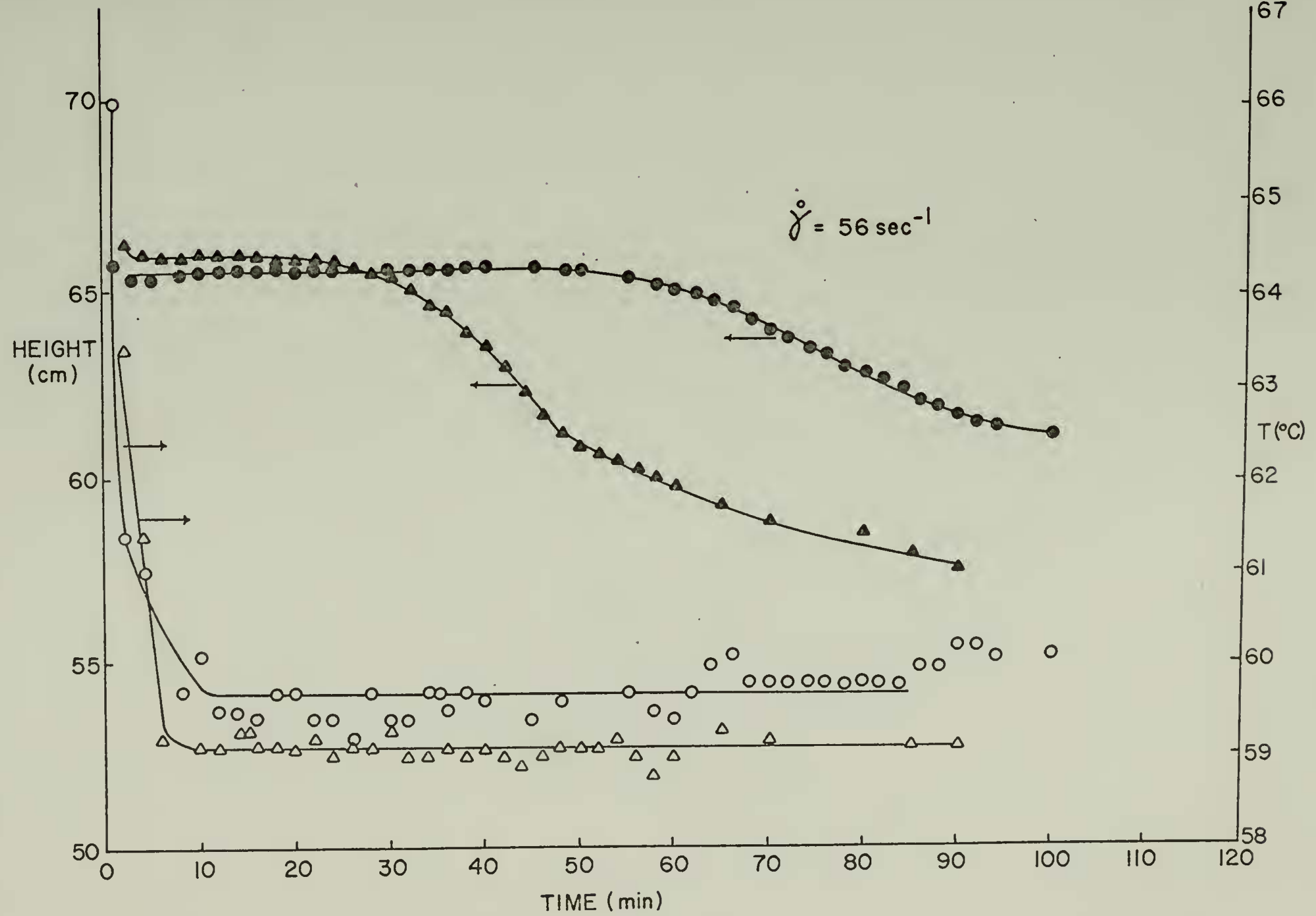
70
65
60
55
50
HEIGHT (cm)
$\dot{\gamma}$ = 56 sec^{-1}
67
66
65
64
63
62
61
60
59
58
T(°C)
0
10
20
30
40
50
60
70
80
90
100
110
120
TIME (min)

A set of crystallization curves are obtained at constant shear rate and at varying temperatures. Figure 9 shows a series of curves of Carbowax 20-M crystallized under 56 sec^{-1} shear. It is desirable to compare crystallization curves at constant temperature and at varying shear rates instead of at varying temperatures and constant shear rate. Therefore, shift factor curves are constructed which allow the crystallization curves at intermediate temperatures to be estimated. Figure 10 gives the shift factors in natural logarithms plotted against the measured temperatures for Carbowax 20-M crystallized under 56 sec^{-1} shear. From this information, the influence of varying shear rates on a polymer crystallized at constant temperature may be compared.

Material

Polyethylenoxide (PEO) is the material selected for this study. It was chosen because it has a low melting point, has one crystal form, and is water soluble.

The crystal form is monoclinic with a 7_2 helix molecular structure.[86,87] The existence of one crystal form is essential. Studies by Wereta and Gogos have shown that shear alters the crystal structure during the crystallization of polybutene-1.[64] These researchers found that shear accelerates the formation of Type 1 (3_1 helix) relative to the formation of Type 2 (11_3 helix).

Figure 9 Series of crystallization curves for Carbowax 20-M crystallized under 56 sec^{-1} shear at varying temperatures, the fraction of crystallinity is plotted versus the natural logarithm of time in minutes

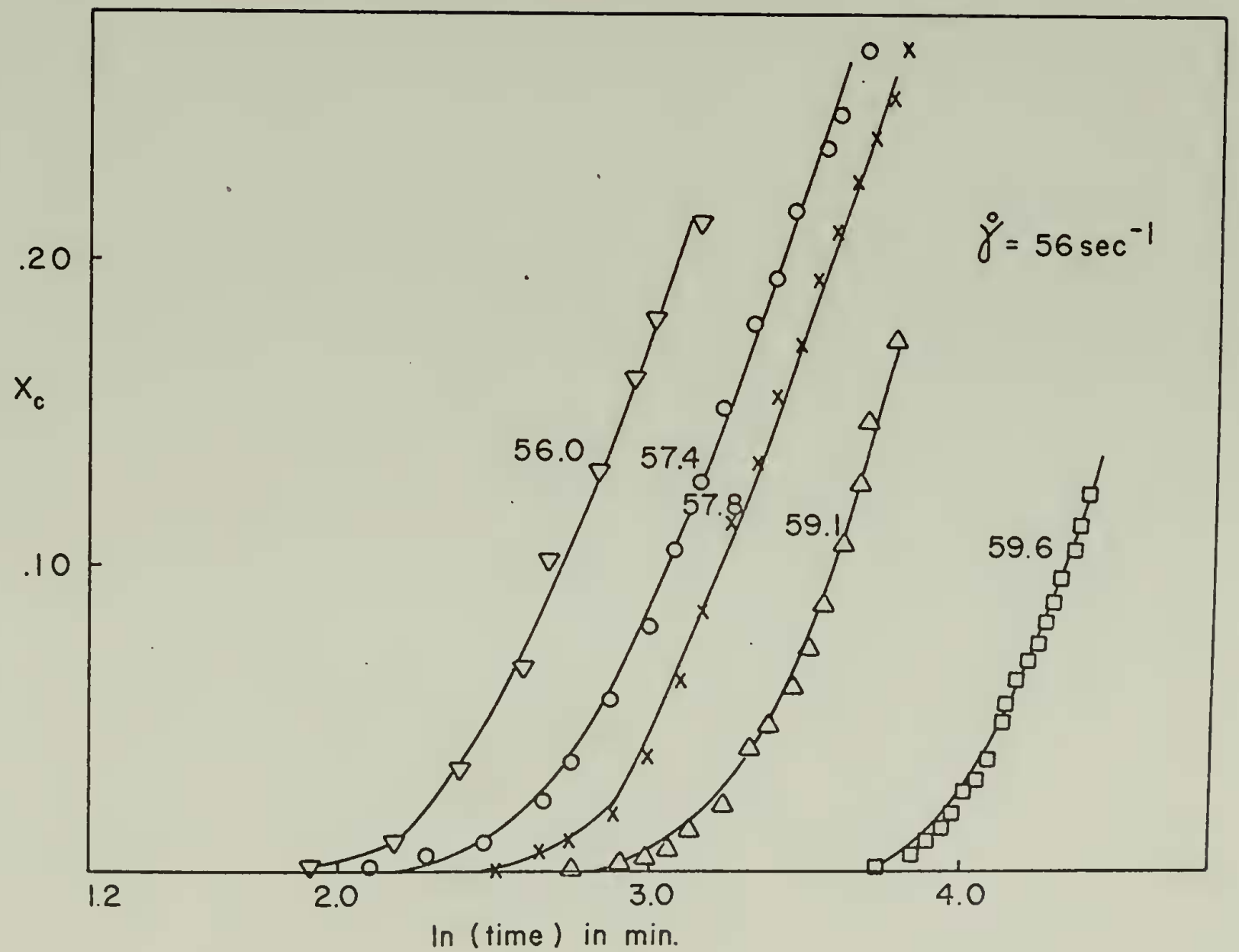
.20
.10
X_c
56.0
57.4
57.8
59.1
59.6
$\dot{\gamma}$ = 56 sec^{-1}
1.2
2.0
3.0
4.0
ln (time) in min.

Figure 10 Shift factor curve for Carbowax 20-M at 56 sec^{-1} shear

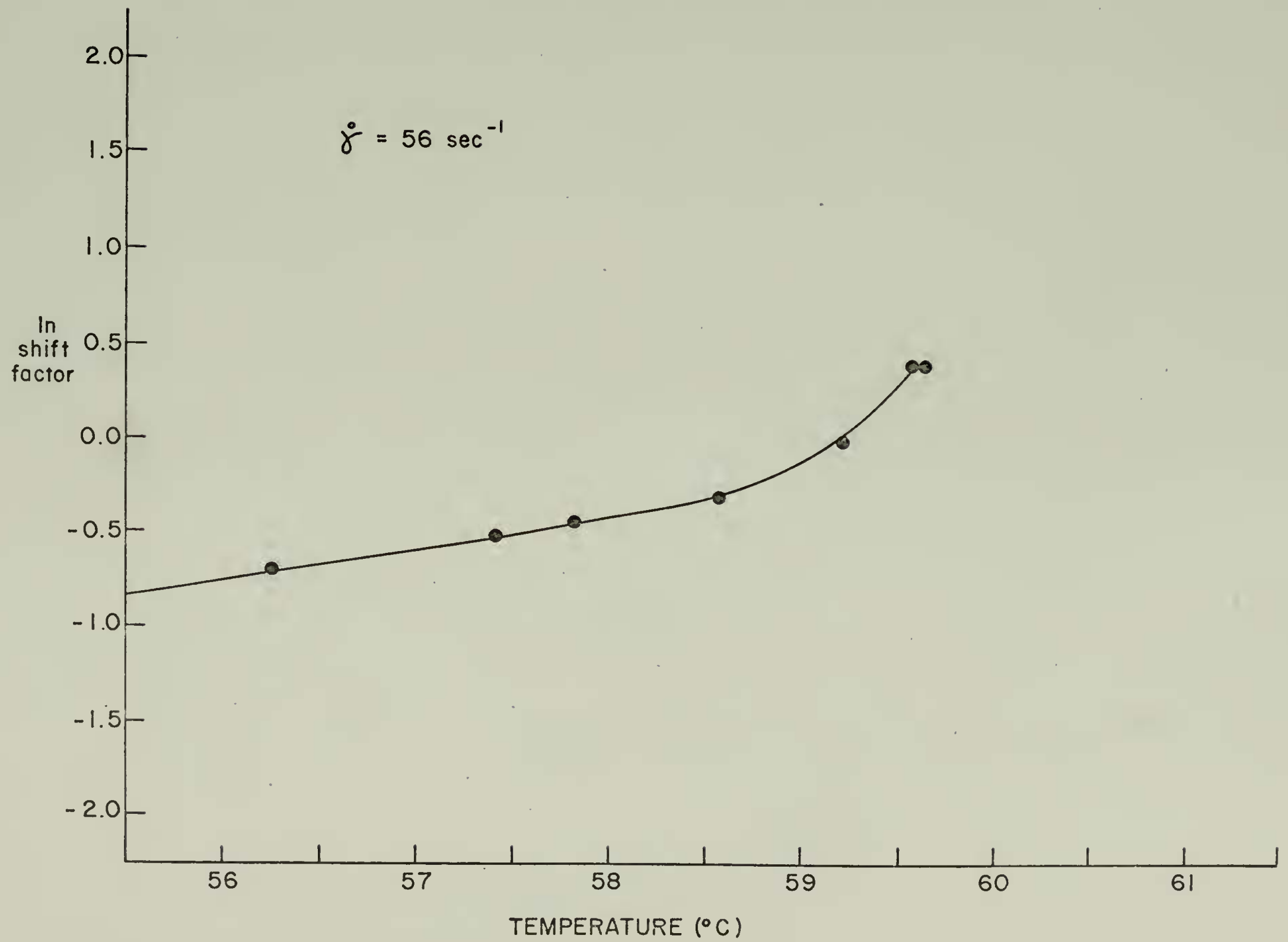
$\dot{\gamma}$ = 56 sec^{-1}
ln shift factor
2.0
1.5
1.0
0.5
0.0
-0.5
-1.0
-1.5
-2.0
56
57
58
59
60
61
TEMPERATURE (°C)

Therefore, selection of any polymer with two or more crystal forms would severely complicate the interpretation of the data.

PEO, however, does exhibit anomalous behavior in crystallization. When PEO is crystallized from thin films, the Maltese cross pattern indicative of true spherulitic structure is present. Crystallization from thick samples produces a birefringent spherical entity in which no Maltese cross pattern is apparent. This, and the light scattering studies of Stein and Rhodes[88], seems to indicate that the large spherical entities grown from thick samples are not true spherulites but rather spherical crystalline aggregates.

The low melting point is important because the polymer is to be melted and crystallized upon mercury. Mercury is highly toxic, and the toxicity rapidly increases with increasing temperature. Because the laboratory in which these experiments were to be undertaken is poorly ventilated, the low melting point of 66°C was important.

The polymer is also water soluble. This property, coupled with its low melting point, increases the ease of cleaning the dilatometer between experiments.

Other advantages possessed by PEO are its relatively low nucleation density and the previous experience with it by this research group. Polyethyleneoxide is also known to exhibit orientation effects.

There is a range of polyethyleneoxides with varying molecular weights available. Those chosen for use in this study were WSR-205, Carbowax 4000, and Carbowax 20-M. These polyethylene glycols are manufactured by the Union Carbide Corporation.

The molecular weight characterizations of the samples were performed by DeBell and Richardson, Inc., of Enfield, Connecticut, on a Waters Associates gel permeation chromatograph. The samples of unsheared Carbowax 20-M and WSR-205 were run in m-cresol at 100 ^{o}C. The presence of a high molecular weight tail in the distribution of Carbowax 20-M was confirmed by first dissolving the sample in benzene to form a highly concentrated solution. This was then diluted with THF to an appropriately low concentration and run through one 10^5 GPC column. The values calculated from the chromatogram as supplied by DeBell and Richardson, are shown in Table 3.

DeBell and Richardson also ran gel permeation chromatographs of the sheared Carbowax 20-M, sheared and unsheared samples of a low molecular weight fraction of Carbowax 20-M, and sheared and unsheared samples of Carbowax 4000. The samples of the sheared material were obtained upon cleaning the dilatometer after each series of crystallization experiments. THF was the solvent. However, no calculations of the molecular weights were performed. Only the calibration curve was provided. The investigator calculated the number

TABLE 3

MOLECULAR WEIGHT DISTRIBUTIONS OF POLYMERS STUDIED

Sample	$\bar{A}_w$*	$\bar{A}_n$*	$\bar{A}_w/\bar{A}_n$	$\bar{M}_w$**	$\bar{M}_n$**
Unsheared, Unfractionated Carbowax 20-M	32,900	2,220	14.8	395,000	26,600
Sheared, Unfractionated Carbowax 20-M	20,700	1,990	10.4	248,000	23,800
Unsheared, Fractionated Carbowax 20-M***	980	525	1.9	11,800	6,300
Sheared, Fractionated Carbowax 20-M***	760	470	1.6	9,200	5,700
Unsheared Carbowax 4000	185	162	1.1	2,200	1,950
Sheared Carbowax 4000	200	169	1.2	2,400	2,030
WSR-205	42,100	3,200	13.19	506,000	38,300

* Angstrom values based on polystyrene standards and toluene.
** Molecular weight based on an assumed equivalance of MW/ A(Å) equal to twelve.
*** The low molecular weight fraction of Carbowax 20-M. The next 43 grams out of a 300 gram sample after 220 grams had been removed.

average and weight average molecular weights from their definitions and the chromatographs.[89] The values determined are also given in Table 3.

The values thus determined, especially the weight average molecular weights, appear to be too small. These differences may arise from the difficulty in estimating the contribution of the high molecular weight chains in the curve. Although these chains may constitute a very small percentage of the total number of chains present, they contribute immensely to the weight average molecular weight. This high contribution results from the squaring of the masses in the weight average molecular weight calculations.

Comparison of the chromatographs yielded little apparent difference between the sheared and the unsheared samples. These curves were almost superimposable. These results indicate that little shear degradation occurred.

The intrinsic viscosities of the PEO samples also yield the same result. These values of the intrinsic viscosities performed in water and the calculated viscosity average molecular weights are given in Table 4. These values also indicate that little shear degradation occurred in the crystallization experiments under shear.

As a final test for shear degradation, crystallization experiments were often done in duplicate. The crystallization curves of fractionated Carbowax 20-M, unfractionated

TABLE 4

INTRINSIC VISCOSITIES AND VISCOSITY AVERAGE MOLECULAR WEIGHTS FOR PEO SAMPLES

Sample	T, °C	$[\eta]$	$\bar{M}_{v}$*
Carbowax 20-M Unfractionated			
Unsheared	42.0	.34	37,000
Sheared	42.0	.35	38,000
Carbowax 20-M Fractionated			
Unsheared	45.0	.13	11,000
Sheared	45.0	.13	11,000
Carbowax 4000			
Unsheared	45.0	.09	7,000
Sheared	45.0	.09	7,000

*Calculated from the appropriate Mark-Houwink constants.[90]

Carbowax 20-M, and Carbowax 4000 obtained at the same temperature and shear rate were superimposable. Several crystallization experiments at the same temperature and shear rate were found which were separated in time by other crystallization experiments. Yet, their crystallization curves were superimposable. This evidence also indicates that little shear degradation occurs during these experiments.

Analysis of the Carbowax 20-M, as supplied by R.R. Kiser of the Union Carbide Corporation, indicates an ash level of 0.96 per cent by weight. An analysis of the same material carried out at the Microanalytical Laboratory at the University of Massachusetts indicates an ash content of 0.90 per cent. Elemental analysis of the residue shows that it is composed entirely of potassium oxide. This indicates that the heterogeneities present in the material consist of catalyst residue since KOH is used in the production of PEO. TGA analysis of Carbowax 20-M showed no volatile material up to 900 ^{o}C other than the products of the polymer decomposition.

CHAPTER V

RESULTS AND DISCUSSION

Samples of unfractionated Carbowax 20-M, fractionated Carbowax 20-M, Carbowax 4000, and a mixture of Carbowax 4000 and WSR-205 were crystallized under shear. The experiments demonstrated that the molecular weight of the polymer as well as the shear rate and the degree of supercooling influence the crystallization kinetics in a sheared melt.

Unfractionated Carbowax 20-M

Table 5 lists the Avrami constants for Carbowax 20-M. These constants were determined from the Taylor's series expansion of the Avrami equation. The Avrami exponent, n, was determined from the slope of the line resulting from the plot of the logarithm of the fraction of crystallinity versus the logarithm of the time in minutes. Such a series of plots is shown in Figure 11 for unfractionated Carbowax 20-M crystallized at a shear rate of 56 sec^{-1}.

The values of the Avrami coefficients listed in Table 5 are only approximate as are those determined for subsequent samples. A least-squares analysis indicated that errors up to 15% exist in the calculated values of ln k.

The last column in Table 5 lists the approximate fraction of crystallinity at which the experimentally determined

TABLE 5

AVRAMI CONSTANTS FOR UNFRACTIONATED CARBOWAX 20-M

Shear Rate Sec^{-1}	Temp. ^{o}C	n	k*	Range X_c
0	54.8	2.7	1.9×10^{-5}	.10
0	55.6	2.6	1.6×10^{-6}	.08
0	56.5	2.7	7.8×10^{-8}	.05
28	58.3	3.7	1.2×10^{-6}	.09
28	58.7	4.2	7.3×10^{-8}	.09
28	59.5	4.9	4.4×10^{-10}	.09
56	56.0	4.3	2.6×10^{-6}	.10
56	57.4	4.4	1.9×10^{-7}	.05
56	57.8	5.6	1.7×10^{-9}	.07
56	59.1	6.4	2.4×10^{-11}	.05
56	59.6	7.0	1.6×10^{-14}	.06
84	58.6	4.3	9.3×10^{-8}	.10
84	59.0	5.0	3.4×10^{-9}	.10
84	59.4	5.6	4.4×10^{-11}	.10
84	60.0	7.7	9.9×10^{-17}	.08
112	56.6	4.4	1.6×10^{-6}	.07
112	58.6	6.6	9.4×10^{-11}	.06
112	59.8	7.3	4.5×10^{-13}	.09
112	60.6	8.4	4.2×10^{-20}	.10

TABLE 5, CONT'D

AVRAMI CONSTANTS FOR UNFRACTIONED CARBOWAX 20-M

Shear Rate Sec-1	Temp. °C	n	k*	Range X_c
140	57.1	4.0	7.2×10^{-7}	.07
140	58.6	4.9	5.9×10^{-9}	.05
140	59.2	6.6	4.0×10^{-12}	.06
140	60.1	6.1	6.8×10^{-13}	.06
168	57.8	4.7	2.3×10^{-8}	.10
168	59.2	4.4	1.2×10^{-8}	.07
168	59.6	9.8	2.6×10^{-19}	.03

---

* The time units in the values of k in this and all subsequent tables are minutes.

Figure 11 Carbowax 20-M crystallized at varying temperatures at 56 sec^{-1} shear rate, log X_c versus log t for Taylor's series expansion of Avrami equation

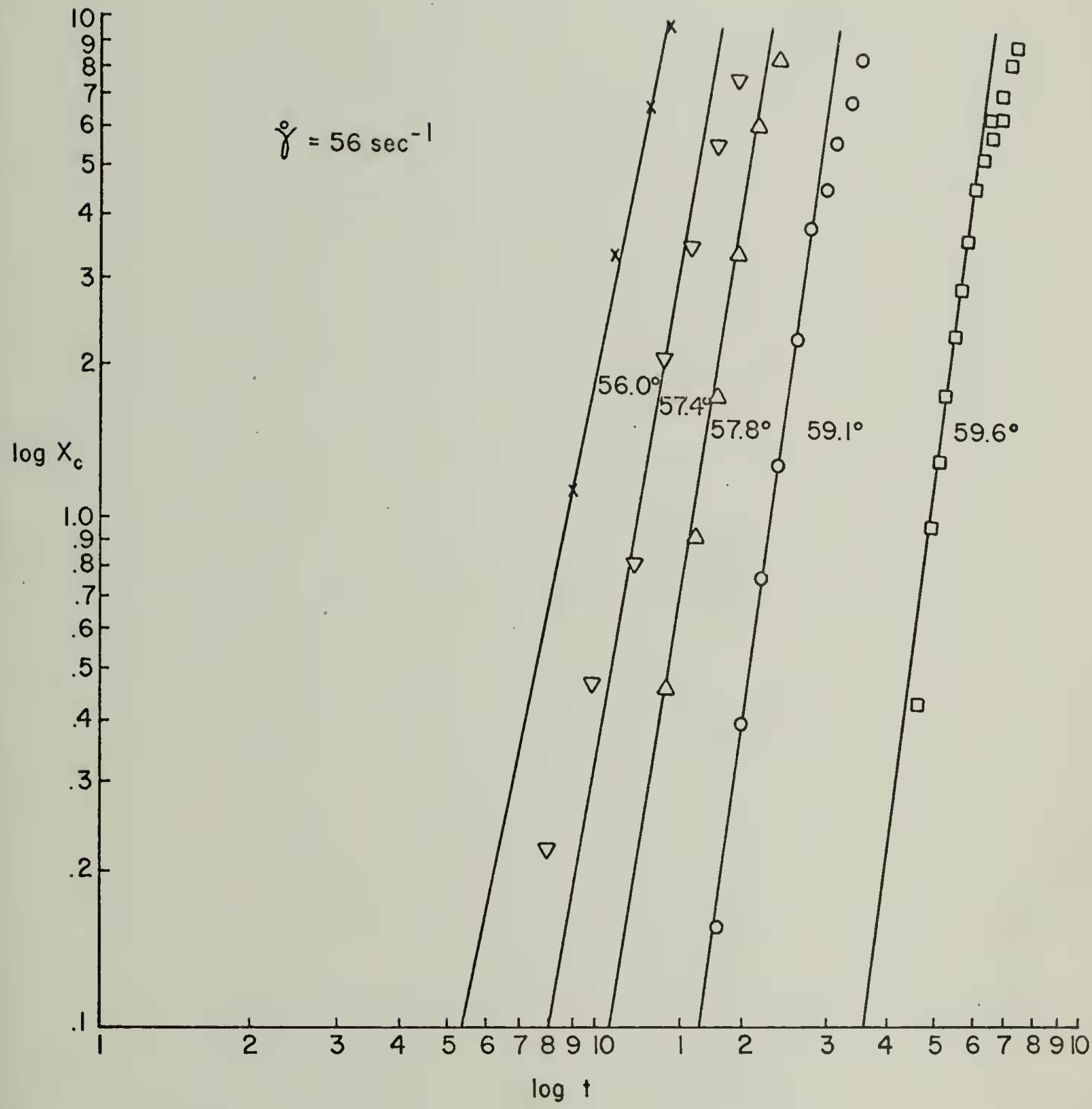
$\dot{\gamma}$ = 56 sec^{-1}
56.0°
57.4°
57.8°
59.1°
59.6°
log X_c
log t
10
9
8
7
6
5
4
3
2
1.0
.9
.8
.7
.6
.5
.4
.3
.2
.1
1 2 3 4 5 6 7 8 9 10 1 2 3 4 5 6 7 8 9 10

values start to deviate from linearity. This deviation results from the temperature gradient which exists across the annulus. It should be noted that degrees of crystallinity above .10 were not considered in the analysis. The crystallization under quiescent conditions are also observed to deviate from linearity. This deviation also results from a temperature gradient across the annulus. This gradient occurs because the thermal fluid is first circulated around the outside of the stationary cylinder before it is channeled into the inner cylinder. The water is several tenths of a degree cooler when it enters the inner cylinder.

The calculated values of the Avrami exponents for the polymer crystallized under quiescent conditions lie within the range of reported values.[20,84,91-94] However, the values of the Avrami exponent for the melt crystallized under shear are higher than those obtained under quiescent conditons and increase with increasing temperature. This change in the Avrami exponent with temperature is depicted graphically in Figure 12. These high values of the Avrami exponent and their increase with temperature are not artifacts of the experiment but must be indicative of the crystallization mechanism. The crystallization model study supports this view. The model shows that the measured values of the Avrami exponent would be less than the real exponent. Therefore, the values of the exponent listed

Figure 12 The change in the Avrami exponent versus temperature for Carbowax 20-M

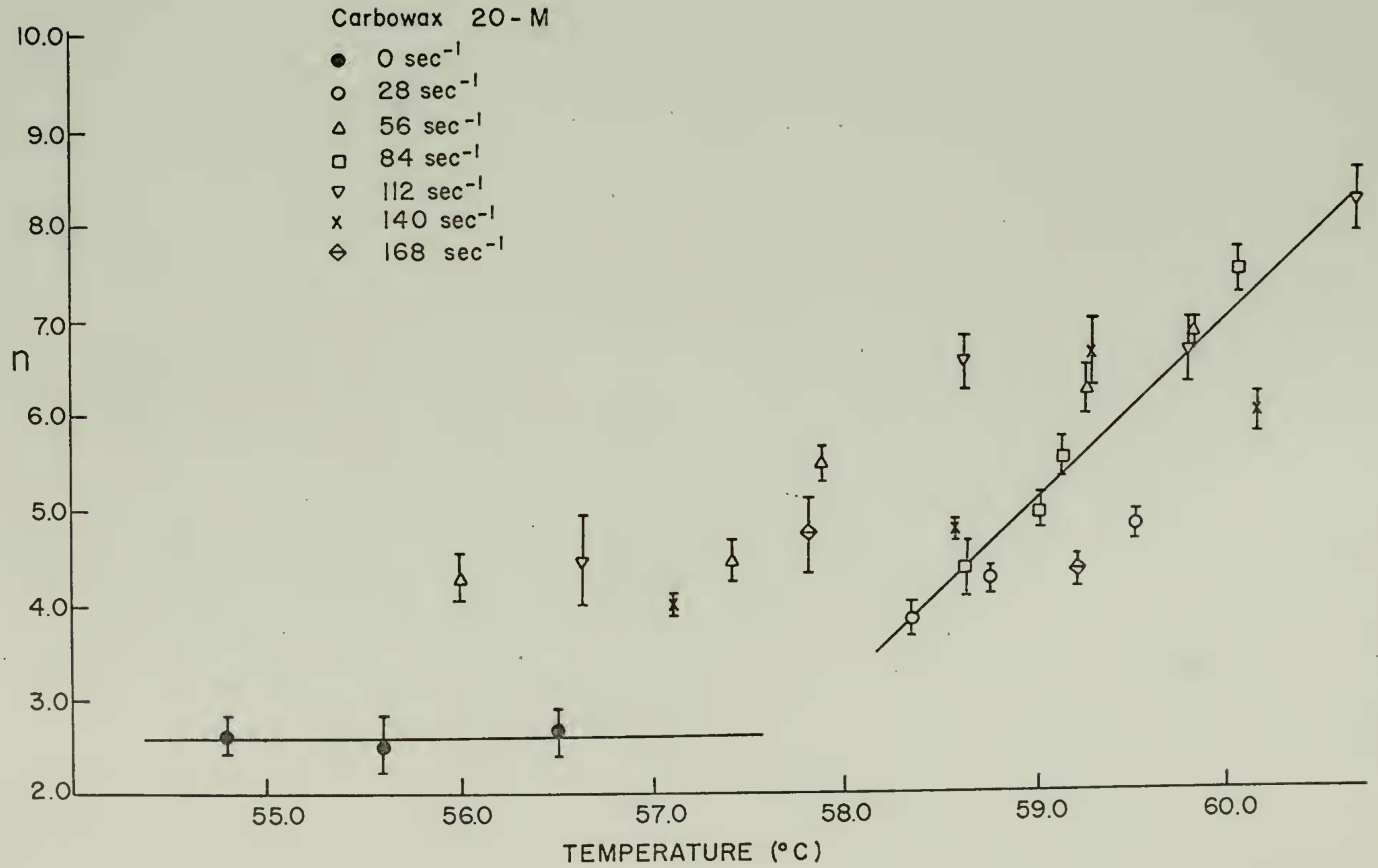
Carbowax 20-M
0 sec⁻¹
28 sec⁻¹
56 sec⁻¹
84 sec⁻¹
112 sec⁻¹
140 sec⁻¹
168 sec⁻¹
n
10.0
9.0
8.0
7.0
6.0
5.0
4.0
3.0
2.0
55.0
56.0
57.0
58.0
59.0
60.0
TEMPERATURE (°C)

in Table 5 are only minimum values. It is also noted that increasing the temperature did not alter the calculated temperature or crystallization profiles. According to the model, the experimental values should not only be less than the real values but should also be independent of temperature. One possible explanation for this phenomenon may be speculated. When a crystalline aggregate is growing in a melt under shear, it is subjected to a stress. This stress not only causes orientation in the melt, but also could cause disruption of these crystalline aggregates. This disruption results in the introduction of more nuclei into the melt as the crystallization proceeds. This disruption also rapidly increases the surface area available for future growth. This "pseudohomogeneous" nucleation yields an apparent increase in the Avrami exponent.

Robert Ulrich observed that shear rate conditions cause the number of particles to be greater than that in the quiescent case at a given fraction of crystalline material.[81] He also noted that the crystalline aggregates appear to break up during shear, but this evidence alone was not sufficient to prove that particle breakup is a controlling factor in the kinetic behavior.

The values of the Avrami exponent, as seen in Figure 12 increase with increasing temperature at constant shear rate. This phenomenon could result from two factors. Both

the viscosity of the amorphous resins and the number of nuclei of critical size decrease with increasing temperature. As the viscosity decrease, the chains slip past one another more easily. Therefore, more stress is absorbed by the crystalline cross-links that do exist in the melt. Yet, as the temperature increases fewer crystalline aggregates exist in the melt because there were fewer nuclei to start them. (The critical sized nucleus necessary to form them is larger than at greater supercoolings and consequently less probable.) Each aggregate would then be subjected to a larger stress and be more readily disrupted. Then each crystalline aggregate would yield more growing particles to the melt than it would at a greater supercooling. Since the sizes of the crystalline aggregates are more sensitive to small changes in the temperature than is the viscosity, the influence of the number of crystalline aggregates on this phenomenon should be much greater.

Crystallization curves at constant temperature and varying shear rates may be compared in Figure 13. In this graph, the fraction of crystallinity is plotted versus the natural logarithm of time in minutes. The 0 sec^{-1} curve has an induction time of approximately 1600 minutes while the crystallization runs under various shear rates have induction times around 16 to 20 minutes. The induction time is the time elapsed between the attainment of thermal equilibrium

Figure 13 Degree of crystallinity versus the natural logarithm of the time in minutes for Carbowax 20-M at 59.0 °C under varying shear rates

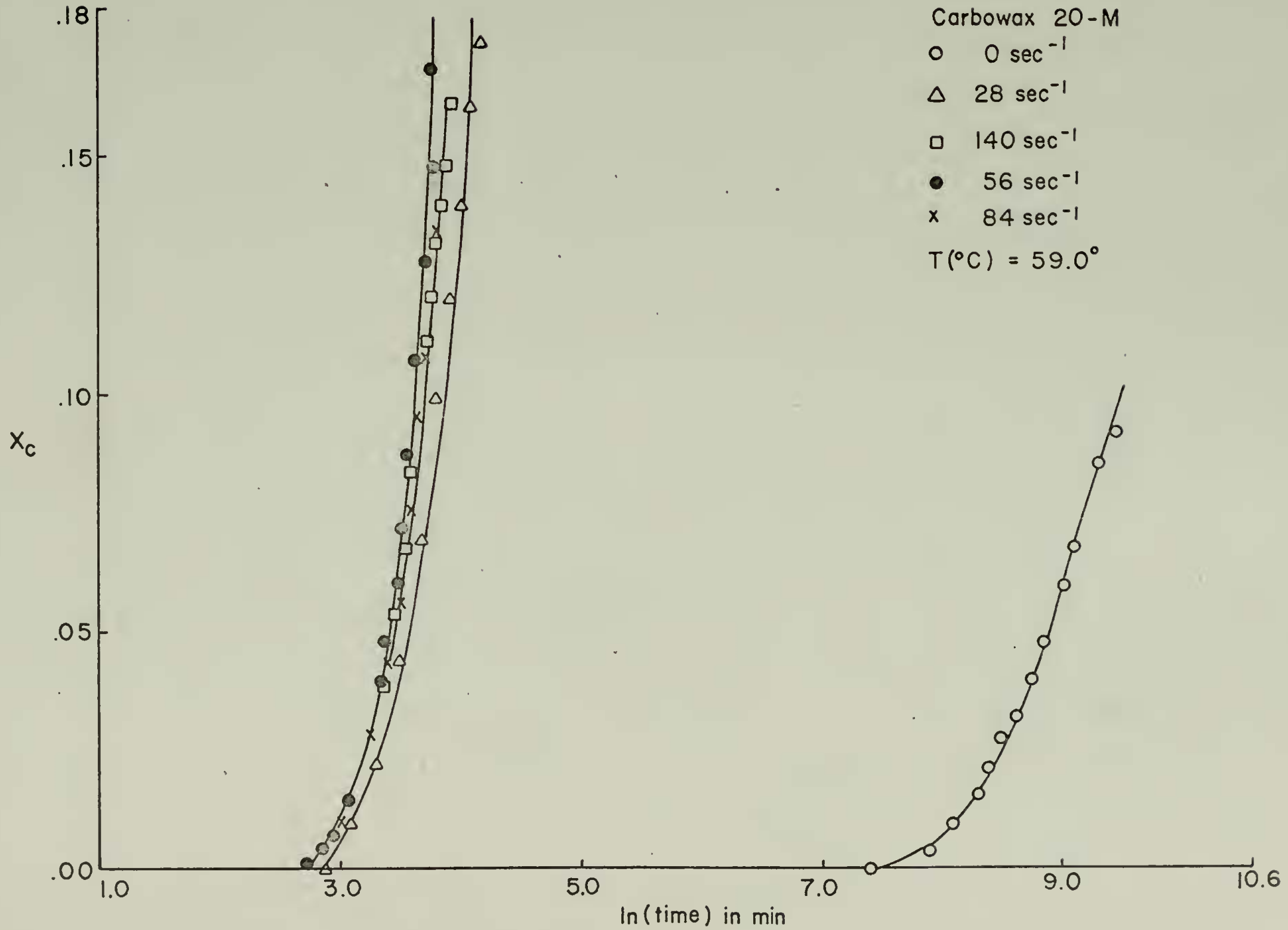
Carbowax 20-M
0 sec⁻¹
28 sec⁻¹
140 sec⁻¹
56 sec⁻¹
84 sec⁻¹
T(°C) = 59.0°
.18
.15
.10
.05
.00
Xc
1.0
3.0
5.0
7.0
9.0
10.6
ln (time) in min

and the appearance of crystallinity. It is readily observed that the crystallization under shear occurs sooner and much more rapidly than it does under quiescent conditions. The small difference in induction times among the sheared crystallization curves suggest that the effect of shear is saturated out over a very narrow range of shear rates. The crystallization curve for Carbowax 20-M under 28 sec^{-1} shear appears only a few minutes later than those at the higher shear rates, and the curves for the higher shear rates superimpose within the experimental error. It would be necessary to shear the melt at lower shear rates to produce intermediate crystallization curves. This procedure is particularly difficult with the reductor in the present set-up because it is difficult to maintain a constant speed at low motor speeds.

Fractionated Carbowax 20-M

It is known that a shorter polymer chain is involved in fewer entanglements than a longer chain. At equal temperatures and shear rates, the shear stress would be less in a lower molecular weight system than in a high molecular weight one. It is this shear stress which orients the polymer chains in the melt and increases the supercooling. It also disrupts growing crystalline aggregates during the crystallization process thus accelerating the transformation.

Therefore, reducing the molecular weight should lower the shear stress at a given shear rate and would be phenomenologically the same as reducing the shear rate in the study of a higher molecular weight system.

The low molecular weight fraction of Carbowax 20-M was provided by R. Ulrich, who used the high molecular weight fraction to raise the shear stress in his studies.[81] The viscosity average molecular weights of the fractionated and the unfractionated Carbowax 20-M samples can be seen and compared in Table 4. The results of a gel permeation chromatography analysis are seen in Table 3.

A series of crystallization curves of fractionated Carbowax 20-M plotted at 56.0°C and at varying shear rates is seen in Figure 14. A series of crystallization curves of the unfractionated Carbowax 20-M at the same temperature is shown in Figure 15 for comparison. In both graphs the crystallization curves for the quiescent transformation appear at the longest induction times, and the sheared transformations appear at shorter induction times. However, in the low molecular weight fraction, the crystallization curves may now be differentiated. The induction time is longer for a melt crystallized at 14 sec^{-1} than for one crystallized at 28 sec^{-1}. The induction time is also longer for a melt crystallized at a shear rate of 28 sec^{-1} than for one crystallized at 140 sec^{-1}. Comparison of Figures 14

Figure 14 Degree of crystallinity versus the logarithm of time for fractionated Carbowax 20-M at 56.0 °C under varying shear rates

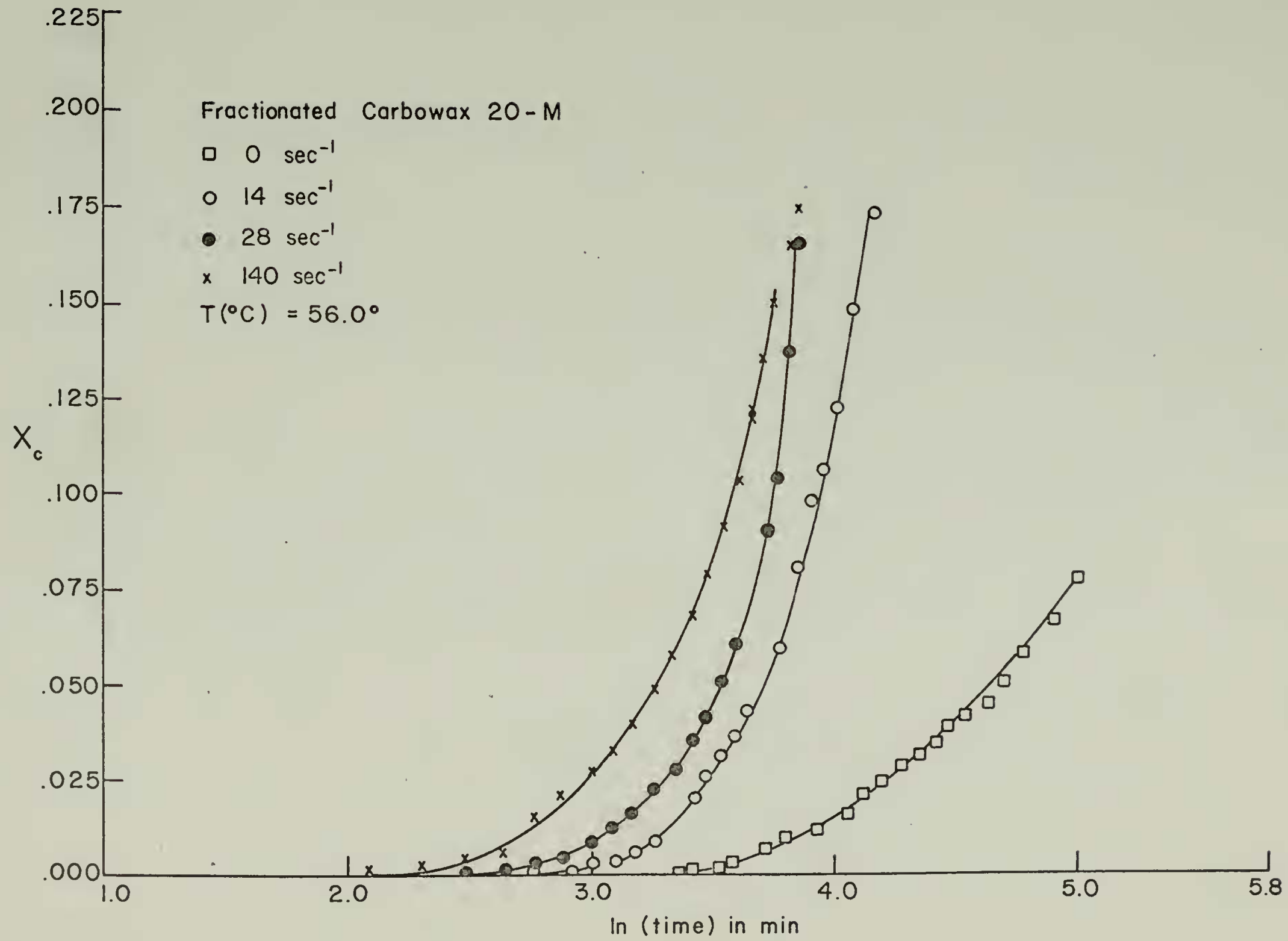
Fractionated Carbowax 20-M
□ 0 sec⁻¹
○ 14 sec⁻¹
● 28 sec⁻¹
x 140 sec⁻¹
T(°C) = 56.0°
X_c
.225
.200
.175
.150
.125
.100
.075
.050
.025
.000
1.0
2.0
3.0
4.0
5.0
5.8
ln (time) in min

Figure 15 Degree of crystallinity versus the logarithm of time for unfractionated Carbowax 20-M at varying shear rates

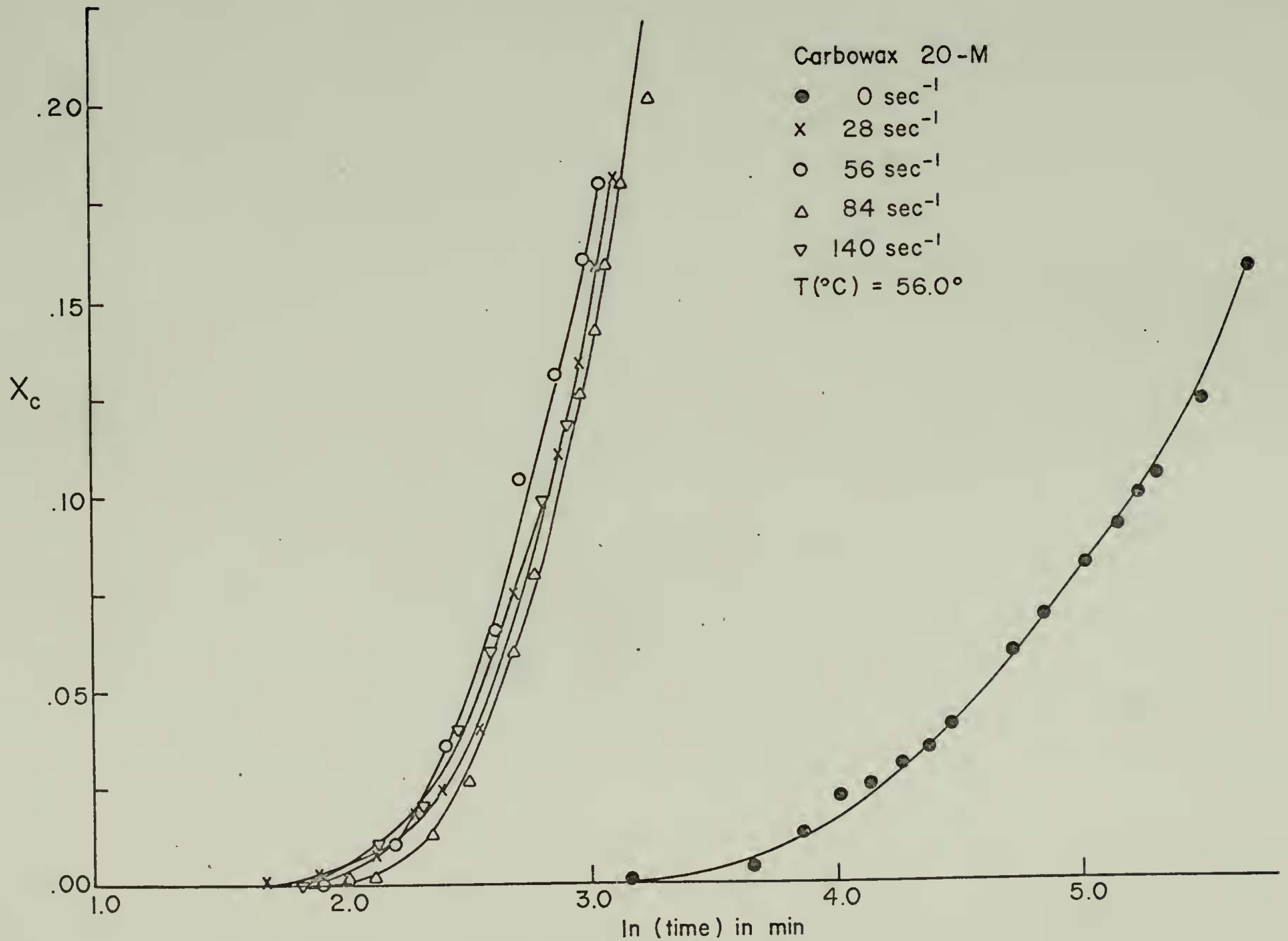
Carbowax 20-M
● 0 sec⁻¹
x 28 sec⁻¹
○ 56 sec⁻¹
△ 84 sec⁻¹
▽ 140 sec⁻¹
T(°C) = 56.0°
.20
.15
.10
.05
.00
X_c
1.0
2.0
3.0
4.0
5.0
ln (time) in min

and 15 also reveals that crystallization occurs sooner and more rapidly for the unfractionated material than for the fractionated material at any given shear rate.

The values of the Avrami constants are listed in Table 6 for the fractionated Carbowax 20-M. It should be noted that the values of the Avrami exponent represent minimum values due to the effect of shear heating and that the values of k are only approximations.

An examination of Table 6 reveals that again the Avrami exponents for quiescent systems are constant with temperature and correlate with the exponents determined by other investigators for polyethyleneoxide.[20,84,91-94] Also, the Avrami exponents of the crystallization transformation under constant shear increase with increasing temperature as previously observed for the unfractionated material. Therefore, it appears that crystallization under shear proceeds by the same mechanism in both the fractionated and unfractionated materials.

Comparison of Tables 5 and 6 shows that crystallization is induced at higher temperatures for the unfractionated material than for the low molecular weight fraction of Carbowax 20-M. This phenomenon is indicative of a greater stress induced supercooling in the unfractionated material at a given shear rate.

TABLE 6

AVRAMI CONSTANTS FOR FRACTIONATED CARBOWAX 20-M

Shear Rate Sec^{-1}	Temp. ^{o}C	n —	k —	Range X_c
0	54.0	2.8	6.1×10^{-6}	.04
0	54.6	2.4	4.6×10^{-6}	.03
0	55.0	3.0	7.4×10^{-8}	.02
0	56.0	3.1	6.7×10^{-8}	.02
0	56.6	3.3	6.0×10^{-9}	.02
14	54.6	2.6	1.4×10^{-5}	.10
14	56.0	5.4	1.7×10^{-10}	.10
14	56.6	5.3	1.1×10^{-10}	.05
14	57.4	5.5	4.9×10^{-11}	.10
28	56.0	3.9	6.2×10^{-8}	.10
28	56.6	4.9	5.8×10^{-9}	.10
28	57.5	4.9	3.3×10^{-11}	.10
28	58.2	8.8	8.8×10^{-21}	.10
140	56.0	3.6	5.0×10^{-7}	.10
140	56.6	5.0	2.3×10^{-11}	.10
140	57.5	5.5	3.9×10^{-13}	.10
140	58.0	5.1	1.1×10^{-13}	.10
140	58.6	7.2	1.5×10^{-23}	.10

Carbowax 4000

Crystallization experiments on fractionated and unfractionated Carbowax 20-M revealed that the crystallization kinetics of a sheared melt depend on molecular weight as well as the degree of supercooling and the shear rate. It was therefore desirable to study a sample of polyethyleneoxide with a molecular weight less than the critical entanglement molecular weight.

Porter and Johnson[95] and Teramoto and Fujita[96] determined the critical entanglement molecular weight of PEO to be approximately 10,000. Therefore, Carbowax 4000 was chosen for this study. The molecular weights and the narrow molecular weight distribution shown in Table 3 demonstrate that the Carbowax 4000 is well below the critical entanglement molecular weight. The calculated viscosity average molecular weight of 7000 is a great deal higher than those arising from the GPC measurements. This discrepency could have arisen from errors in the Mark-Houwink constants or from inadvertently neglecting the contribution of a small fraction of high molecular weight component in the GPC calculations. Still all values indicate a molecular weight less than the critical entanglement molecular weight.

Although the polymer molecules composing the melt are less than the critical entanglement molecular weight,

orientation occurs under shear. The chains are subject to less stress than in a higher molecular weight sample, but not all the chains will readily slip past one another.

The Avrami constants calculated for the crystallization transformations of Carbowax 4000 are presented in Table 7.

Examination of Table 7 reveals that the values of the Avrami exponent are again higher than those determined for the quiescent crystallizations. However, they appear to be more shear rate sensitive and less temperature sensitive than those determined for Carbowax 20-M samples. It is readily apparent that the values of the Avrami exponent increase with increasing shear rate.

Figures 16, 17, 18, and 19 show crystallization curves for Carbowax 4000 at 52°, 53°, 54°, and 55°C., respectively. Examination of Figure 16 reveals that the sheared crystallization curves appear at the same induction time. In all the figures, the time interval between the appearance of the quiescent crystallization curve and the crystallization curve with the shortest induction time is approximately constant. The crystallization curves in Figure 16 show that the transformation at the 56 sec^{-1} shear rate is initially more rapid than the others. It also shows that the transformation at 28 sec^{-1} is initially more rapid than that at 140 sec^{-1}. As the temperature is increased, increased separation between the crystallization curves occurs.

TABLE 7

AVRAMI CONSTANTS FOR CARBOWAX 4000

Shear Rate Sec^{-1}	Temp. C	n —	k —	Range X_c
0	51.3	3.3	5.0×10^{-8}	.10
0	51.6	3.9	2.2×10^{-9}	.10
0	53.0	3.5	2.3×10^{-9}	.07
0	54.0	3.2	2.3×10^{-9}	.02
28	51.6	3.2	5.2×10^{-6}	.10
28	52.5	3.6	2.3×10^{-7}	.10
28	54.0	3.4	2.0×10^{-8}	.10
28	54.6	3.8	1.5×10^{-9}	.10
56	51.4	2.9	1.5×10^{-5}	.10
56	53.0	5.1	3.3×10^{-10}	.10
56	54.0	4.1	1.0×10^{-9}	.10
56	55.0	4.8	3.9×10^{-11}	.08
140	51.3	5.0	1.8×10^{-8}	.10
140	53.1	6.2	2.9×10^{-12}	.10
140	54.1	6.4	1.2×10^{-14}	.06
140	55.0	6.4	2.2×10^{-17}	.06

Figure 16 Degree of crystallinity versus the logarithm of time for Carbowax 4000 at 52.0°C. at varying shear rates

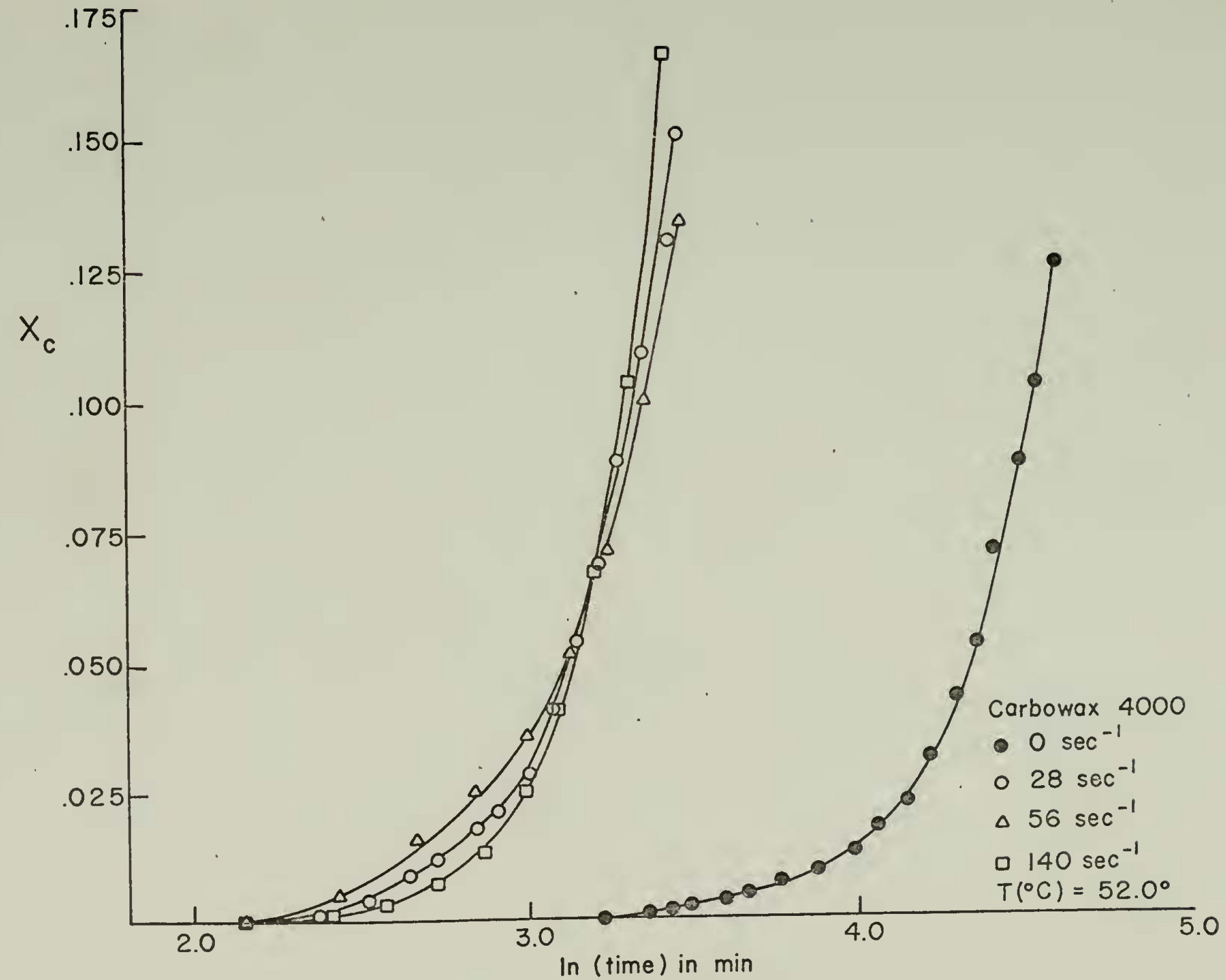
.175
.150
.125
X_c
.100
.075
.050
.025
2.0
3.0
4.0
5.0
ln (time) in min
Carbowax 4000
0 sec^{-1}
28 sec^{-1}
56 sec^{-1}
140 sec^{-1}
T(°C) = 52.0°

Figure 17 Degree of crystallinity versus the logarithm of time for Carbowax 4000 at 53.0°C at varying shear rates

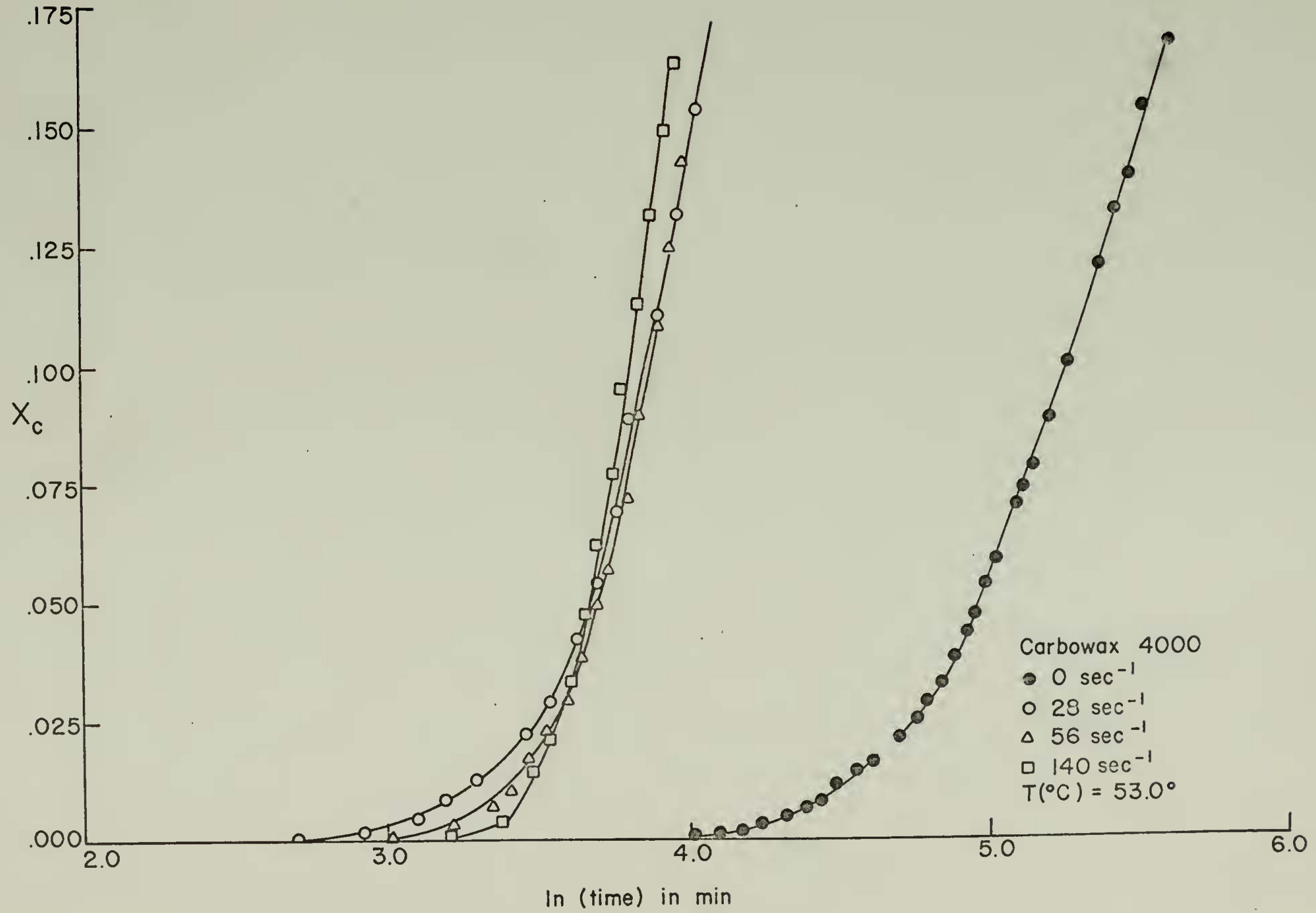
.175
.150
.125
.100
X_c
.075
.050
.025
.000
2.0
3.0
4.0
5.0
6.0
ln (time) in min
Carbowax 4000
0 sec^{-1}
28 sec^{-1}
56 sec^{-1}
140 sec^{-1}
T(°C) = 53.0°

Figure 18 Degree of crystallinity versus the logarithm of time for Carbowax 4000 at 54.0 °C at varying shear rates

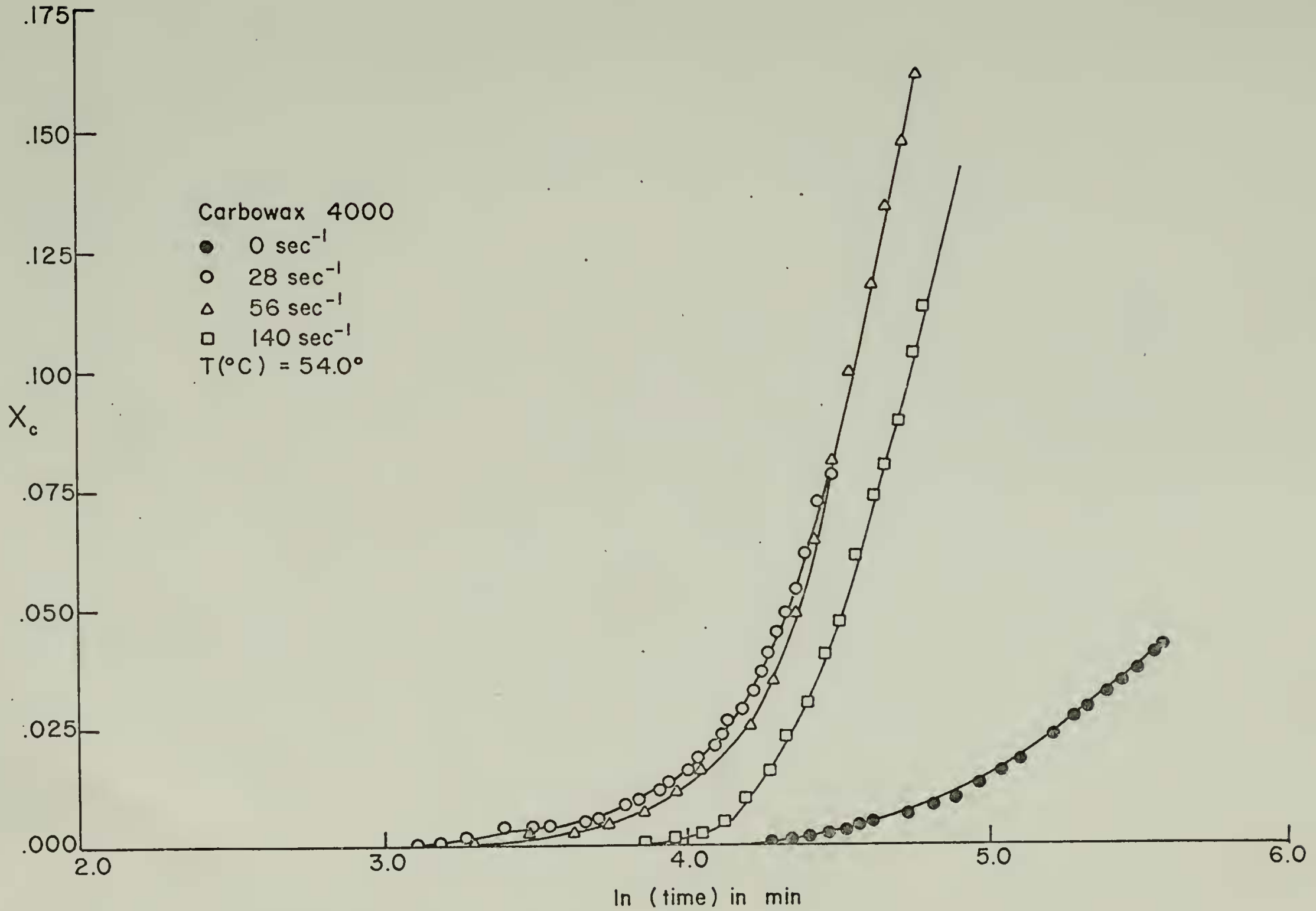
.175
.150
.125
.100
.075
.050
.025
.000
X_c
Carbowax 4000
0 sec^{-1}
28 sec^{-1}
56 sec^{-1}
140 sec^{-1}
T(°C) = 54.0°
2.0
3.0
4.0
5.0
6.0
ln (time) in min

Figure 19 Degree of crystallinity versus the logarithm of time for Carbowax 4000 at 55.0°C and at varying shear rates

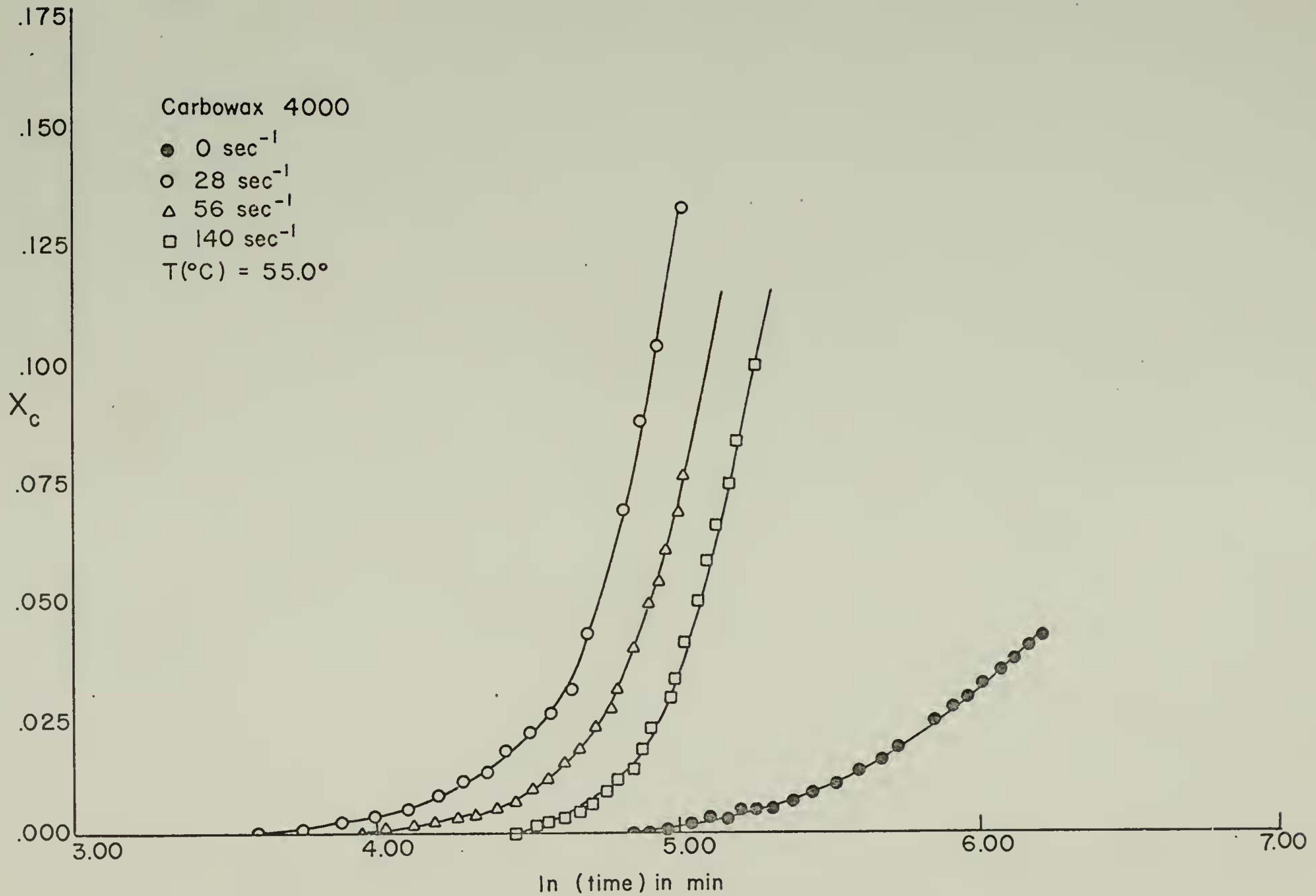
Carbowax 4000
0 sec⁻¹
28 sec⁻¹
56 sec⁻¹
140 sec⁻¹
T(°C) = 55.0°
.175
.150
.125
.100
.075
.050
.025
.000
Xc
3.00
4.00
5.00
6.00
7.00
ln (time) in min

In the crystallization curves at 53.0°C. seen in Figure 17, the induction times of the curves are in exactly the reverse order of what would have been anticipated from the experiments with Carbowax 20-M. The induction time is the shortest for Carbowax 4000 crystallized at a shear rate of 28 sec^{-1}. The induction time for the melt crystallized at a 56 sec^{-1} shear rate is longer than that for 28 sec^{-1}. The longest induction time is observed in the melt crystallized at a shear rate of 140 sec^{-1}. Increasing the temperatures of crystallization further separate these crystallization curves. The effect is most dramatically seen in Figure 19 for crystallization at 55.0°C. Each crystallization curve is distinctly separated with the lowest shear curve appearing at the shortest induction time and the highest shear curve appearing at the longest induction time.

These observations may be explained from three factors which control the appearance of crystallization in a sheared melt. The factors are the temperature sensitivity of the nucleation and growth rates, the orientation of the melt under stress, and the slippage of the chains past one another under shear.

As the supercooling is increased in the temperature range under consideration the primary and secondary nucleation rate is increased. Therefore, more crystalline tie-points are formed in the melt in a given period of time. Also more of the melt is transformed in a given interval at

a lower temperature than would be transformed at a higher temperature.

The orientation of the chains under stress reduces the change in entropy between the melt and the crystal. This reduction of the entropy results in an increase in the degree of supercooling. Therefore, increased shear should accelerate the crystallization transformation.

Prior to any crystallization, all the tiepoints are formed by entanglements of the polymer chains. These initial entanglements are temporary in nature. The length of time which they exist depends upon the temperature, molecular weight, and the shear rate. As the temperature and the shear rate increase, the polymer chains slip more readily past one another. The entanglements exist for a shorter duration. However, as the molecular weight of the chains increase, the lifetime of the entanglements also increases.

The slippage of the chains past one another is very fast below the critical molecular weight for entanglements. The rate of slippage increases with increasing shear rate. Although orientation occurs in the melt under shear, increasing shear disrupts regions of high order in the melt by removing the more highly oriented chains in this region. Therefore, the chain slippage retards the formation of critical sized nuclei for spontaneous growth. This in turn retards the appearance of crystallization.

Therefore, the influence of supercooling and orientation is to accelerate crystallization, but the influence of chain slippage is to delay it.

In each case studied, the quiescent crystallization appears at longer induction times than does crystallization in the sheared regimes. The effect of orientation induced by shear is to accelerate crystallization at all temperatures. However, increasing the temperature reduces the nucleation and growth rates of the crystalline aggregates. The critical radius necessary for spontaneous growth is increased by increasing temperature. Yet, the increase in shear at constant temperature would increase the slippage of the chains thereby increasing the difficulty of forming critical sized nuclei. Therefore, the higher shear rates although inducing higher orientation would also induce higher slippage. This retardation of crystallization is much higher at higher temperatures because the radius needed for the critical sized nuclei is so much larger and the viscosity is less.

Similar observations were made by Porter and Johnson in studies on partially crystalline polyethylene.[97] The polyethylene used by Porter and Johnson also had a molecular weight below that needed for critical entanglement. They observed in intermediate shear, defined as less than 10,000 sec^{-1} in a capillary rheometer, that the viscosity increased

with decreasing shear. From these observations they concluded that crystalline aggregates were disrupted and crystallite formation was retarded under shear.

Further examination of Figures 16 and 17 reveals that the crystallization curves cross over one another. The crystallization curves for the higher shear rates have a higher rate of increase than the lower. This indicates that the growing crystalline aggregates are disrupted creating surfaces for further nucleation as postulated in the discussion of the Carbowax 20-M experiments. The acceleration or retardation of the transformation depends primarily upon the size of the fractured portions of the crystalline aggregate. The portions which are still larger than the critical sized nucleus continue to grow. Those smaller disappear.

One would then predict a decrease in the number of nuclei at low degrees of crystallization transformation and an increase of nuclei at more extensive degrees of crystallinity. The examination of the surface after crystallization microscopically would also yield smaller, more numerous particles in the sheared cases than in the unsheared. Both observations were reported by R. Ulrich.[81]

Mixture of Carbowax 4000 and WSR-205

It has been observed that at constant temperature

decreasing the molecular weight decreased the time difference between the appearance of crystallization in the quiescent and the sheared systems. For instance, the induction time differences between the sheared curves and the unsheared curve of unfractionated Carbowax 20-M are greater than those of the fractionated material. The quiescent and sheared crystallization curves of Carbowax 4000 appear even closer together. If decreasing the molecular weight of the sample moves the sheared crystallization curves to longer induction times, then the addition of a small amount of a very high molecular weight polymer to a low molecular weight polymer should increase the crystallization rate of the mixture relative to the low molecular weight component.

To test this hypothesis a 4.76 per cent mixture of WSR-205 in Carbowax 4000 was made by first dissolving 2.5491 grams of WSR-205 and 50.9859 grams of Carbowax 4000 in benzene. The polymer mixture was then separated from solution by freeze drying to insure a homogeneous mixture of the two components. As seen in Table 3, the WSR-205 has a weight average molecular weight of 506,000 and a number average molecular weight of 38,300. The distribution is wide with $\overline{M}_w/\overline{M}_n$ equal to 13.19.

The acceleration of the appearance of crystallization by addition of the WSR-205 is shown in Figure 20. Here are displayed the crystallization curves of both Carbowax 4000

Figure 20 Degree of crystallinity versus the logarithm of time for Carbowax 4000 and a mixture of Carbowax 4000 and WSR-205 at 53.0 ^{o}C, crystallized at 0 sec^{-1} and 28 sec^{-1}

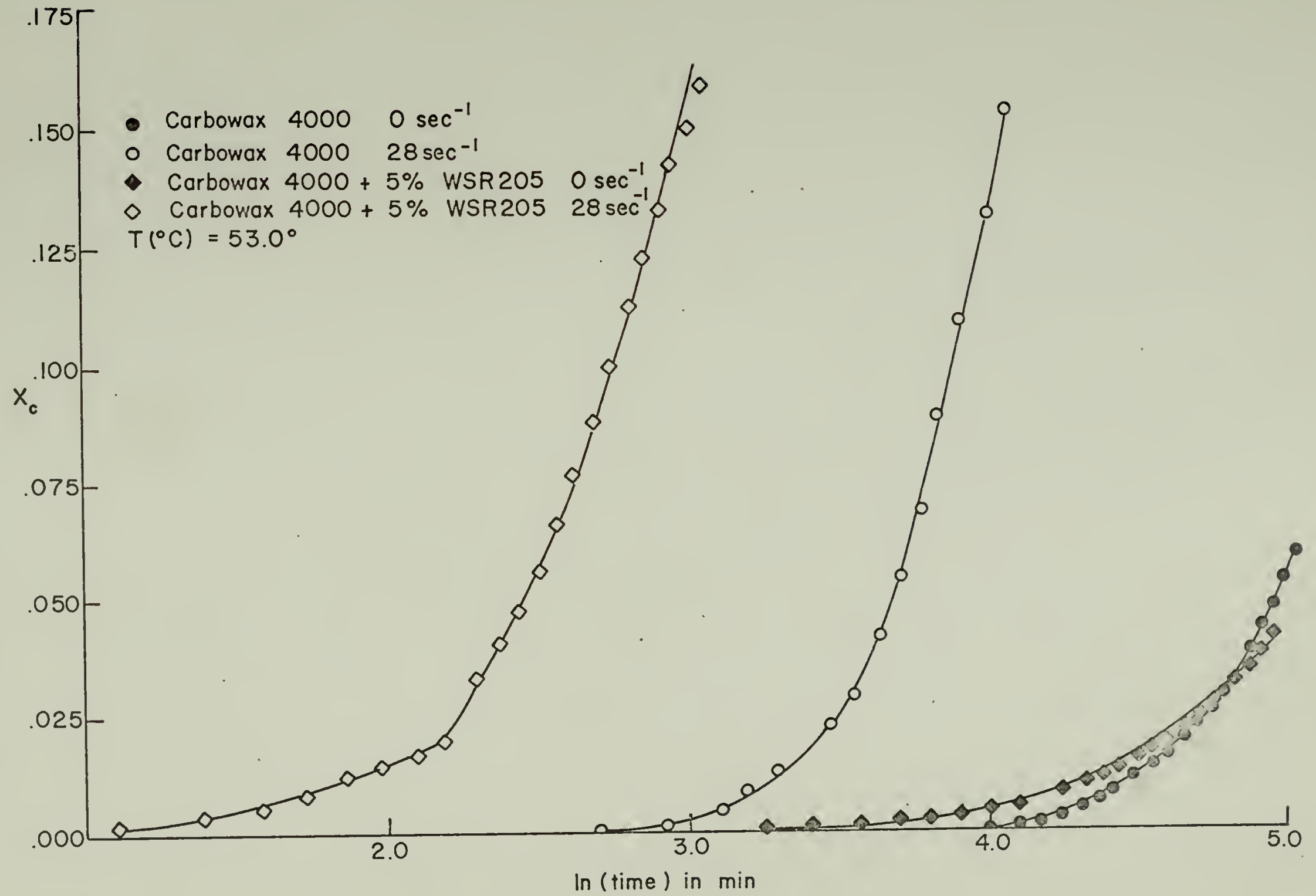
Carbowax 4000 0 sec⁻¹
Carbowax 4000 28 sec⁻¹
Carbowax 4000 + 5% WSR205 0 sec⁻¹
Carbowax 4000 + 5% WSR205 28 sec⁻¹
T(°C) = 53.0°
.175
.150
.125
.100
.075
.050
.025
.000
Xc
2.0
3.0
4.0
5.0
ln (time) in min

and the mixture of Carbowax 4000 and WSR-205 at 0 sec^{-1} and 28 sec^{-1}. The crystallization curves for both are quite similar under quiescent conditions. However, the crystallization curve for the sheared mixture of Carbowax 4000 and WSR-205 has a much shorter induction time than does the curve for the Carbowax 4000 alone.

The high molecular weight WSR-205 component is more highly oriented by shear than the Carbowax 4000, and it supports most of the shear stress in the melt. This higher orientation increases the supercooling in the melt.

It is possible that only the local supercooling in the melt around the high molecular weight chains is increased. Then the WSR-205 would crystallize first followed later by the Carbowax 4000. After repeated crystallizations, the previously homogeneous melt may be partially fractionated. Keith and Padden postulated that during spherulitic growth the low molecular weight material is trapped in the interfibrillar layers.[98,99] This process would lead to a reduction in the observed values of the Avrami exponent. Hay and coworkers also observed that in crystallizing PEO samples with very broad molecular weight distributions under quiescent conditions, the Avrami exponent drops very rapidly from 3.0 to values of 1.8 to 2.0.[93]

The values of the Avrami exponents determined for the mixture of Carbowax 4000 and WSR-205 are given in Table 8. The values of the Avrami coefficient have been omitted from

TABLE 8

AVRAMI EXPONENTS FOR THE MIXTURE OF CARBOWAX 4000 AND WSR-205

Shear Rate Sec-1	Temp. C	n —	Range X_c
0	49.5	2.7	.05
0	53.0	2.6	.05
0	53.9	3.5	.05
28	53.9	2.4	.10
28	55.1	2.2	.02
56	53.1	2.1	.07
56	54.1	2.7	.02
140	53.1	1.9	.04
140	53.9	2.1	.06

this table because the sheared crystallization curves were not reproducible. Repeated crystallization under shear shifted the crystallization curves made at the same shear rate and temperature to longer induction times. This indicates that shear degradation may be occurring in this system. This is not too surprising when it is considered that most of the shear stress is carried by the small fraction of WSR-205 chains present. Therefore, this system is more susceptible to degradation than the other systems studied.

The crystallization curve displayed in Figure 20 was the first sheared crystallization made after those crystallizations performed under quiescent conditions. So the position of the curve for the mixture crystallized at 28 sec^{-1} is more accurate than those curves derived from later crystallizations under shear. Still, Figure 20 dramatically illustrates the influence of a high molecular weight component on polymer crystallization under shear.

CHAPTER VI

CONCLUSIONS

It has been shown by this research that the kinetics of crystallization of uncrosslinked melts of polyethylene-oxide are altered by shearing. At constant temperature and shear rate, the induction time of the crystallization curve is influenced by the molecular weight of the polymer. It was found that in moderate to high molecular weight samples, the effect of shear becomes saturated at very low shear rates. Decreasing the molecular weight decreases the shear stress in the melt. This decrease in shear stress is the same as reducing the shear rate and separates the crystallization curves. The curves from the highest shear rate appear at the shortest induction time.

Further decreasing of the molecular weight to below that of the critical entanglement molecular weight allows the nucleation rate, strongly dependent upon the supercooling, to influence the relative positions of the sheared crystallization curves. Although the sheared crystallization curves always appear at shorter induction times than the quiescent crystallization runs, at fixed temperature the highest shear rates give the smallest induction times only at the greatest supercooling. At lower supercoolings, low shear rates give smaller induction times than do high

shear rates. It is postulated that at small degrees of supercooling the nuclei are disrupted more readily than at high degrees of supercooling. Therefore, it is more difficult to attain a critical sized nucleus which may grow spontaneously.

A distribution of embryos may be envisioned as a function of size. As the size of the embryo increases, the number of embryos decreases. Shear distorts the embryo distribution relative to the quiescent case. A decrease is seen in the number of embryos of a given size as the shear rate is increased. This decrease is a function of the molecular weight as well as the shear rate. The distortion is less at high molecular weights than at low molecular weights. At low molecular weights, the chains slip past one another more readily than at high molecular weights. At high shear rates, the chains also slip past each other more rapidly. Therefore, high shear rates on chains below the critical entanglement length may retard the onset of crystallization relative to low shear rates.

Once the embryo reaches a size at which it can grow spontaneously, two possibilities may occur. The crystalline aggregate may be broken into portions larger or smaller than the critical sized nucleus.

Disruption of a growing particle into portions smaller than critical size causes it to disappear. This effect

of disruption is greater at lower supercoolings than at higher supercoolings. At a larger supercooling, not only is the growth rate of the crystalline aggregates faster, but the critical sized nucleus necessary for spontaneous growth is smaller. Therefore, when a growing crystalline aggregate is disrupted, it is less likely to be broken into fragments whose sizes are below that necessary for a critical sized nucleus.

The influence of nucleation is important in low molecular weight chains because of the higher stress relaxation rates relative to high molecular weight chains. In high molecular weight chains the slippage of the chains past each other is retarded both by the entanglements and the growing crystalline aggregates which function as cross-links. In low molecular weight polymers, only the crystalline aggregates serve to reduce the stress relaxation, and any disruption of these aggregates will serve to increase the slippage of the polymer chains.

If the crystalline aggregate is broken into portions larger than the critical sized nucleus, these particles will persist in the melt. They will also continue to grow spontaneously. Thus, a "pseudo-homogeneous" process occurs with the continuous infusion of growing particles into the melt. This infusion is reflected by abnormally high values for the Avrami exponent. These high values for the Avrami

exponent were detected in all the molecular weight ranges studied.

The values of the Avrami exponent increase with decreasing supercooling at constant shear rate. This phenomenon may result from the decrease in both the viscosity and the number of nuclei with increasing temperature. As the viscosity decrease, the chains are able to slip past one another more easily. Therefore, more of the stress is absorbed by the crystalline cross-links in the melt. Yet, as the temperature increases fewer crystalline aggregates exist in the melt because the critical sized nucleus necessary to form them is larger than at greater supercoolings. Each aggregate would then be subjected to a larger stress and be disrupted more easily. Then each crystalline aggregate would yield more growing particles to the melt than it would at greater supercooling. The influence of the number of crystalline aggregates on this phenomenon should be much greater than the viscosity. The sizes of the crystalline aggregates are more sensitive to small changes in the temperature than is the viscosity.

The concept of crystalline aggregate disruption increasing the number of growing particles to accelerate the crystallization transformation yields several suggestions for further research. Polyethyleneoxide is a brittle

material. It is not a structural material used for fabrication under high shear. Nor does it form true spherulites but crystalline aggregates. Its crystallization behavior under shear may be atypical of polymers. It is important to measure the crystallization kinetics of other polymers under shear to determine if their crystallization transformations proceed by the same mechanism.

The molecular weight has been shown to be of considerable importance in influencing the crystallization transformation behavior under shear. A series of studies on narrow well-defined fractions of polymer would be enlightening. The influence of increasing molecular weight on the appearance of the crystallization transformation curves could be more closely monitored. The positions of the saturation of the effect of shear on crystallization could then be determined as a function of molecular weight. A decrease in the shear rate needed for the appearance of saturation would be expected with increasing molecular weight.

It is also desirable to study the region between the crystallization under quiescent conditions and those shear rates which lead to saturation in moderate to high molecular weight polymers. This region could be investigated with the addition of a new reductor which further reduces the speed of rotation of the inner cylinder. A study in the

shear rate domain of 1-10 sec^{-1} should yield interesting results.

As the crystallization transformation proceeds, the shear stress increases. It is desirable to be able to monitor this increase by addition of a strain gauge to the dilatometer.

The crystallization experiments described in this thesis were undertaken over a very narrow range of supercoolings. The large thermal mass of the dilatometer and the small size of the thermostatting system required long times for the establishment of thermal equilibrium. The relative positions of the sheared crystallization curves of PEO with molecular weights below the critical entanglement length vary at different degrees of supercooling. At the lowest temperatures, the induction time for the highest shear rate crystallization was the least. At higher temperatures the lowest shear rate crystallization appeared at the shortest induction time. This phenomenon was attributed to the influence of the highly temperature sensitive nucleation rates and distortion of the embryo distributions by shear. This temperature sensitivity may also influence the crystallization behavior of longer chains. The influence of nucleation rate on the crystallization behavior of high molecular weight polymers would have to be studied at small degrees of supercooling.

In order to extend the range of the instrument to greater supercoolings, the dilatometer must be modified. A larger range of supercoolings may be obtained by substituting aluminum for stainless steel in the construction of the inner and outer cylinders. The aluminum has a much greater thermal conductivity than stainless steel and is also relatively inert to chemical attack. The heating system can be improved by removing the copper coils surrounding the outer cylinder and placing it instead in contact with a large fluid reservoir maintained at the appropriate temperature.

Finally, the dilatometer is assembled by screwing the outer cylinder into the stationary head. This method of assembly has several disadvantages. The gasket is distorted by twisting. The outer cylinder must be secured very tightly to prevent leakage which makes the instrument extremely difficult to disassemble. The condition can be rectified by removing the screw threads and using bolts to secure the outer cylinder to the head. The tightening of the bolts will cause compression of the gasket without the twisting. Also, the instrument will be more easy to disassemble.

LITERATURE CITED

1. B. Wunderlich, J. Polymer Sci. A, 1, 1245 (1963).

2. B. Wunderlich and T. Arakawa, ONR Report No. 6, Contract Nonr. 401 (44), 491 (19), Task No. 051-428.

3. B. Wunderlich and T. Arakawa, J. Polymer Sci. A, 2, 3697 (1964).

4. P.H. Geil, F.R. Anderson, B. Wunderlich, and T. Arakawa, J. Polymer Sci. A, 2, 3707 (1964).

5. F. Gornick and J.D. Hoffman, Ind. Eng. Chem., 58, 41 (1966).

6. F. P. Price, J. Polymer Sci., 42, 49 (1960).

7. J.I. Lauritzen and J.D. Hoffman, J. Res. Natl. Bur. Std., 64A, 1 (1960).

8. J.I. Lauritzen and J.D. Hoffman, J. Res. Natl. Bur Std., 64A, 73 (1960).

9. J.D. Hoffman and J.I. Lauritzen, J. Res. Natl. Bur. Stds., 65A, 297 (1961).

10. D. Turnbull and J.C. Fisher, J. Chem. Phys., 17, 71 (1949).

11. F. Von Goler and G. Sachs, Z. Physik, 77, 281 (1932).

12. M Avrami, J. Chem. Phys., 7, 1103 (1939).

13. M. Avrami, J. Chem. Phys., 8, 212 (1940).

14. M. Avrami, J. Chem. Phys., 9, 177 (1941).

15. U.R. Evans, Trans. Faraday Soc., 41, 365 (1945).

16. L. Mandelkern, Crystallization of Polymers, McGraw-Hill, New York, 1964.

17. A. Sharples, Polymer, 3, 250 (1962)

18. F.P. Price, J. Appl. Phys., 36, 3014 (1965).

19. W. Banks and A. Sharples, J. Polymer Sci. A, 2, 4059 (1964).

20. W. Banks and A. Sharples, Makromol. Chem., 59, 223 (1963).

21. A. Peterlin, J. Appl. Phys., 35, 75 (1964).

22. W. Banks, J.N. Hay, A. Sharples, and G. Thompson, Polymer, 5, 163 (1964).

23. P.H. Till, J. Polymer Sci., 24, 301 (1957).

24. A. Keller, Phil. Mag., 2, 1171 (1957).

25. E. W. Fischer, Z. Naturforsch., 12a, 753 (1957).

26. P.H. Geil, Polymer Single Crystals, John Wiley & Sons, Inc., New York, 1963.

27. D. C. Bassett and A. Keller, Phil. Mag., 7, 1553 (1962).

28. A. Keller and A. O'Connor, Discussion Faraday Soc., 25, 114 (1958).

29. F.P. Price, J. Chem. Phys., 35, 1884 (1961).

30. B.G. Ranby, F.F.Morehead, and N.M.Walter, J. Polymer Sci., 44, 349 (1960).

31. B.G. Ranby and H. Brumberger, Polymer, 1, 399 (1960).

32. P.H. Geil, N.K.J. Symons, and R.G. Scott, J. Appl. Phys., 30, 1516 (1959).

33. V.F. Holland and P.H. Lindenmeyer, J. Polymer Sci., 57, 589 (1962).

34. A. Keller and D.C. Bassett, J. Roy. Microscope Soc., 79, 243 (1960).

35. R. Jaccodine, Nature, 176, 305 (1955).

36. D. H. Reneker and P. H. Geil, J. Appl. Polymer Sci., 31, 1916 (1960).

37. W. O. Statton and P. H. Geil, J. Appl. Polymer Sci., 3, 357 (1960).

38. J. Willems, Discussions Faraday Soc., 25, 111 (1958).

39. J. Willems and I. Willems, Experientia, 13, 465 (1957).

40. E. W. Fischer, Kolloid-Z., 159, 108 (1958).

41. P. H. Lindenmeyer, S. P. E. Trans, 4, 1 (1964).

42. A. Keller, Kolloid-Z., 165, 15 (1959).

43. D. A. Blackladder and H. M. Schleinitz, Nature, 200, 773 (1963).

44. F. P. Price, General Electric Report No. 67-C-097, March 1967.

45. A. J. Pennings, and A. M. Kiel, Kolloid-Z., 205, 160 (1965).

46. A. J. Pennings, J. Polymer Sci. C, 16, 1799 (1967).

47. A. J. Pennings, J. M. A. A. van der Mark, and H. C. Booij, Kolloid-Z., 236, 99 (1970).

48. B. Wunderlich, C. M. Cormier, A. Keller, and M.J. Machin, J. Macromol. Sci. B, 1, 93 (1967).

49. Geil, Polymer Single Crystals, chap. 4.

50. A. Keller, J. Polymer Sci., 17, 291 (1955).

51. F. P. Price, J. Polymer Sci., 37, 71 (1959).

52. G. E. Ashby, Preprint 27B, Symposium of Effects of Molecular Orientation on Structures and Properties of Polymers, Part I, Pittsburgh, Pa., May 7-10, 1964, Sponsored by AIChE.

53. A. K. Van der Vegt and P.P.A. Smit, Paper No. 17, Symposium on Advances in Polymer Science and Technology, London, May 3-5, 1966, Sponsored by The Society of Chemical Industry.

54. J. H. Southern and R. S. Porter, J. Macromol Sci.-Phys., B4, 541 (1970).

55. J. H. Southern and R. S. Porter, J. Appl. Polymer Sci., 14, 2305 (1970).

56. C. R. Desper, J. H. Southern, R. D. Ulrich, and R. S. Porter, J. Appl. Phys., 41, 4284 (1970).

57. A. Keller and M. J. Machin, J. Macromol. Sci. B, 1, 41 (1967).

58. H. D. Keith, F. J. Padden, and R. G. Vadimsky, J. Polymer Sci. A, 4, 267 (1966).

59. H. D. Keith, F. J. Padden, and R. G. Vadimsky, J. Appl. Phys., 37, 4027 (1966).

60. R. B. Williamson and W. F. Bussi, J. Appl. Phys., 38, 4187 (1967).

61. K. Kobayashi and T. Nagasawa, How Sheared Melts of Polymers Behave in the Crystallization Process, Institute for Chemical Research, Kyoto University, 1968.

62. M. J. Hill and A. Keller, J. Macromol. Sci. B3, 1, 153 (1969).

63. T. W. Haas and B. Maxwell, Polymer Sci. and Eng., 9, 225 (1969).

64. A. Wereta and C. G. Gogos, Polymer Sci. and Eng., 11, 19 (1971).

65. T. Kawai, R. Kamoto, K. Ehara, T. Matsumoto, and H. Maeda, Sen-I Gakkaishi, 26, 80 (1970).

66. V. G. Baranov, Faraday Disc., 1B, 327 (1970).

67. P. J. Flory, J. Chem. Phys., 15, 397 (1947).

68. W. R. Krigbaum and R. J. Roe, J. Polymer Sci. A, 2, 4391 (1964).

69. J. D. Ferry, Viscoelastic Properties of Polymers, John Wiley & Sons, New York, 1961.

70. A. N. Gent, Trans. Faraday Soc., 50, 521 (1964).

71. E. H. Andrews, Proc. Roy. Soc., A271, 562 (1964).

72. H. G. Kim and L. Mandelkern, J. Polymer Sci. A2, 6, 181 (1968).

73. A. J. Chompff and J. A. Duiser, J. Chem. Phys., 45, 1505 (1966).

74. A. J. Chompff and W. Prins, J. Chem. Phys., 48, 235 (1968).

75. P. E. Rouse, Jr., J. Chem. Phys., 21, 1272 (1953).

76. P. G. de Gennes, J. Chem. Phys., 55, 572 (1971)

77. Precision O-Rings, Precision Rubber Products Corporation, 1966.

78. S. Middleman, The Flow of High Polymers, Interscience, New York, 1968, p. 36.

79. R. M. Turian and R. B. Bird, Chem. Eng. Sci., 18, 689 (1963).

80. K. H. Hellewege, R. Hoffman, and W. Knappe, Kolloid-Z., 226, 109 (1968).

81. R. Ulrich, Ph.D. Thesis, University of Massachusetts, Amherst, Mass. (1972).

82. Handbook of Chemistry and Physics, Chemical Rubber Publishing Co., Cleveland, Ohio, 1960, p. 2434.

83. S. Middleman, private communication.

84. W. J. Barnes, W. G. Leutzel, and F. P. Price, J. Phys. Chem., 65, 1743 (1961).

85. F. Danusso and G. Gianotti, Makromol. Chem., 61, 139 (1963).

86. F. P. Price and R. W. Kilb, J. Polymer Sci., 57, 395 (1962).

87. H. Tadokoro, Y. Chatani, T. Yoshishara, S. Tahara, and S. Murahashi, Makromol. Chem., 73, 109 (1964).

88. R. S. Stein and M. B. Rhodes, J. Appl. Phys., 31, 1873 (1960).

89. P. J. Flory, Principles of Polymer Chemistry, Cornell University Press, Ithaca, 1953, pp. 266-314.

90. Polymer Handbook, Editors J. Brandrup and E. H. Immergut, Interscience, New York, 1966.

91. L. Mandelkern, F. A. Quinn, and P. J. Flory, J. Appl. Phys., 25, 840 (1954).

92. N. L. Jain and F. L. Swinton, Eur. Polym. J., 3, 371 (1967).

93. J. N. Hay, M. Sabir, R. L. T. Steven, Polymer, 10, 187 (1969).

94. J. N. Hay and M. Sabir, Polymer, 10, 203 (1969).

95. R. S. Porter and J. F. Johnson, Trans. Soc. Rheol., 6, 107 (1962).

96. A. Teramoto and H. Fujita, Makromol. Chem., 85, 261 (1965).

97. R. S. Porter and J. F. Johnson, Trans. Soc. Rheol., 11, 259 (1967).

98. H. D. Keith and F. J. Padden, J. Appl. Phys., 35, 1270 (1964).

99. H. D. Keith and F. J. Padden, J. Appl. Phys., 35, 1286 (1964).